Fermi National Accelerator Laboratory

FERMILAB-Pub-84/53-E
7190.497
(Submitted to Phys. Rev.)

SEARCH FOR HEAVY CHARGED PARTICLES AND LIGHT NUCLEI AND ANTINUCLEI PRODUCED BY 400 GeV PROTONS

J. L. Thron, T. R. Cardello, P. S. Cooper, L. J. Teig, and Y. W. Wah
J. W. Gibbs Laboratory, Yale University, New Haven, Connecticut 06511

C. Ankenbrandt, J. P. Berge, A. E. Brenner, J. Butler, K. Doroba, J. Elias
J. Lach, P. Laurikainen, J. MacLachlan, and J. P. Marriner
Fermi National Accelerator Laboratory, Batavia, Illinois 60510

E. W. Anderson and A. Breakstone
Iowa State University, Ames, Iowa 50011

and

E. McCliment
University of Iowa, Iowa City, Iowa 52242

June 1984

Search for Heavy Charged Particles

and

Light Nuclei and Antinuclei Produced by 400 GeV Protons

J. L. Thron[†], T. R. Cardello[*], P. S. Cooper,

L. J. Teig and Y. W. Wah[¶]

J. W. Gibbs Laboratory, Yale University, New Haven, CT 06511

and

C. Ankenbrandt, J. P. Berge, A. E. Brenner, J. Butler, K. Doroba[††],

J. Elias, J. Lach, P. Laurikainen[**], J. MacLachlan and J. P. Marriner

Fermi National Accelerator Laboratory, Batavia, IL 60510

and

E. W. Anderson and A. Breakstone

Department of Physics, Iowa State University, Ames, IA 50011

and

E. McCliment

Department of Physics, University of Iowa, Iowa City, IA 52242

The results of a search for heavy charged particles are presented. The experiment was sensitive to particles of mass 4 to 12 GeV/c^2 having lifetimes $\geq 3\times10^{-9}$ seconds. No particles of this type were observed, allowing a new limit of 10^{-36} ($cm^2GeV^{-2}nucleon^{-1}$) to be placed on the invariant production cross section. In addition, the production of the deuteron, antideuteron, triton and He^3 were measured using the same apparatus.

I. Introduction

We report on a search performed at Fermilab, E-497, to look for the existence of new, massive ($\geq$ 4 GeV/c^2) charged particles. The experiment was performed in a negative 86 GeV/c secondary beam produced by 400 GeV/c protons incident on a copper target. The relatively short length of the experiment, less than 20 m from the production target to the final detector, using Čerenkov counters with a momentum analyzed beam, allowed direct electronic observation of new particles with short lifetimes. Previous direct measurement searches[1,2,3,4] using time of flight measurements to determine the particles' velocities required long flight paths (230 to 1100m) to achieve separation of different particles. A similar search[5] for massive, neutral particles used a flight path of 590m with a calorimeter to determine timings and particle energies. Although most of the data were taken using a negative secondary beam of 86 GeV/c momentum, data were also taken at lower momenta where the production of known nuclei were within the detection range of our apparatus. Some data were also taken with a positive secondary beam. The complete set of runs is shown in Table I.

In this experiment, Čerenkov counters were used to reject low mass particles. The momenta of the remaining particles were calculated by observing their deflection by a magnetic field. Their velocities were measured by a Čerenkov counter. These values along with their measured momenta enabled their masses to be calculated.

Theoretical and experimental motivations exist for searching in this lifetime-mass region. Among the suggested particles are massive integrally charged quarks[6, 7], quixes[8], six quark states[9] and pineuts[10]. Calculations for the lightest supersymmetric particles containing gluinos indicate[11,12] that

their lifetime and mass might be in the sensitive range of this experiment. In addition, there have been persistent reports[13,14] of massive charged particles observed in cosmic ray time of flight experiments.

To calibrate the particle search experiment and also since it is of interest in its own right, the production of known particles was also measured. Most of these data were the observation of antideuterons. Their production rate relative to pions was measured and, after correcting for their relative absorptions[15], a production cross section was determined. This can be compared to a number of other measurements[16,17] at various Feynman x and transverse momenta. Similar, but less accurate accurate production measurements were made for deuterons, tritons and He^3.

II. Experimental Apparatus

A. Beam, Target, Channel

This experiment was performed in the Fermilab Proton Center beamline using an incident beam of 400 GeV/c protons. The proton beam was focused to a size of less than 1x1 mm^2 at the target. The incident protons were delivered to the experiment during a 1 second beam pulse with a repetition rate of approximately 10 seconds. The primary beam rate limit of 4.0×10^{10} particles/pulse in this experiment was set by the instantaneous secondary beam rate in the proportional wire chambers (PWCs).

The copper target was 2 mm by 2 mm in cross section. For most runs, it was one absorption length (14.8 cm) long and was mounted so that it could be moved completely out of the beam remotely. The target was centered in the entrance aperture of a 7 m long curved magnetic channel. The channel deflected the secondary beam by 21 mrad and is depicted in Fig. 1. The first section of the

channel (198 cm) contained the target and a beam dump region. The dump absorbed particles emitted by the target which were not in the channel phase space as well as any uninteracted beam particles. The channel walls defined the beam phase space and were made of sintered tungsten (90%W, 6% Ni, 4% Cu) having a density of 17.08 g/cm^3. In this geometry, the angle of the incident proton beam was adjusted so that the central ray corresponded to zero mrad particle production.

The channel was in a 7.0x3.0x1.7 m^3 (lxwxh) dipole magnet. At maximum current the magnet produced a field of 35 kG in the region of the channel. By varying the current and polarity of the magnet, one could select singly charged particles of either sign with momenta up to 350 GeV/c exiting the channel. This system produced a secondary beam with a full width momentum spread of $\Delta p/p = \pm 7\%$ and a solid angle of 0.64 μsr. A more detailed discussion of the channel design and construction is given by Cardello[18].

About 500,000 particles per pulse were normally maintained within the secondary beam phase space. Total rates two to three times higher than this were observed when all the particles passing through the apparatus were included. This excess was mainly due to muons coming through the magnet iron and low momentum particles being produced by interactions of the beam in the walls of the downstream sections of the channel.

B. Proportional Wire Chambers and Scintillation Counters

The trajectories of particles exiting the channel were determined by two clusters of PWCs before the spectrometer magnet and two following it. These are shown in Fig. 2 as PWCs A-D. Clusters A, B and D had wire planes which gave a position measurement in the X (horizontal), Y (vertical) and U (45 degrees)

directions; the C chamber had only X and Y planes. The wire planes in the A, B and C clusters had an effective wire spacing of 203 μm. This was accomplished by using a pair of planes each with 406 μm spacing staggered with respect to each other. Cluster D had only single planes of 406 μm spacing in X and Y. Nineteen wire planes were contained in the total system. The effective area of the chambers was contained in a 2.5 cm diameter circle. The measured resolution of these chambers is consistent with the expected value of the effective wire spacing divided by $\sqrt{12}$. These chambers were capable of handling particle rates up to ≈1MHz.

Three plastic scintillation counters B1, B2 and B3, matched to the size of the PWCs further defined beam particles spatially as well as temporaly. Additional scintillation counters (not shown in Fig. 2) were used in anti-coincidence to reject particles outside the expected beam phase space. These included four counters on the upstream face of the C2 Čerenkov counter to reject particles which would pass through the more sensitive part of its phototubes. Two other counters with holes sufficiently large for the beam to pass through them (called halo counters) insured that beam particles passed through the active area of the PWCs. Finally, four other scintillation counters which could be remotely positioned into the beam proved useful as diagnostic tools.

C. Čerenkov Counters

Four Čerenkov counters were used to tag particles as heavy or light; a fifth actually measured their velocity. These counters fell into three categories: threshold counters (C1,C4) giving a signal for low mass particles, dual channel counters (C3, C5) which could produce a separate signal for either low or high mass particles and a broadband counter (C2) to measure the

particle's velocity. Combining this with momentum information determined the mass of the particle. The Čerenkov counter positions are shown in Fig. 2.

1. Threshold Čerenkov Counter, C1

The C1 Čerenkov counter (Fig. 2) used the last 75 cm of the channel as its radiating volume. This volume was sealed with 1 mil aluminum windows, and Freon (dichloro-tetrafluoro ethane, $C_2Cl_2F_4$) gas at atmospheric pressure flowed through it. At the downstream end, outside of the channel, an aluminized plastic film reflected the Čerenkov radiation via an aluminized light pipe onto a high sensitivity (RCA 31000M) photomultiplier. The light pipe was long enough to ensure that the phototube was in a region of low magnetic field. Two outputs were taken from the base of the phototube. One was used for the fast trigger logic and the other was analyzed by an analog to digital converter (ADC). The threshold for Čerenkov radiation for this counter was a particle with a relativistic γ of 18.6, corresponding to a pion momentum of 2.6 GeV/c.

2. Threshold Čerenkov Counter, C4

The threshold counter, C4, was designed to reject pions. The radiating gas was N_2 at 65 psia, which set the threshold mass at 3.75 GeV/c^2. The counter was mounted on the downstream end of the spectrometer magnet and extended into the magnet aperture.

Figure 3 shows a sectional view of C4. The beam entered through a stainless steel window (0.08 gm/cm^2), traversed the radiating medium (0.75 gm/cm^2) and exited through a final window. The Čerenkov radiation was reflected from a 45° planar mirror onto a spherical mirror at the top of the vertical section. The spherical mirror focused the Čerenkov radiation back through a hole in the center of the 45° mirror onto a quartz lens just before the (RCA 31000M)

photomultiplier. The quartz lens, coated with 54 nm MgF_2, served both as a pressure seal window and a final focusing element. All mirrors were coated with 100 nm aluminum and 25 nm MgF_2. At the operating pressure, the mean Čerenkov angle for pions was 50 mrad.

3. Dual Channel Counters, C3 and C5

The dual channel counters C3 and C5, shown in Fig. 4, were designed to be sensitive to Čerenkov radiation from particles with mass up to 6 GeV/c^2 at beam momenta of 75 GeV/c. The 100 cm long radiating medium was nitrogen at 173 psia and was adjusted to place the discrimination cut between high and low mass channels at 4 GeV/c^2. C3 was mounted on the upstream face of the spectrometer magnet with part of the counter extending into the magnet field. C5 was placed at the end of the experimental beam line. The entrance and exit windows were 25 μm stainless steel. After passing through a thin area in the 45 degree planar mirror, the beam entered the radiating volume. Light produced here was focused by a 48 in focal length spherical (primary) mirror coated with 100 nm aluminum and 25 nm MgF_2.

The Čerenkov radiation, after reflection by the 45° mirror, was brought to a ring focus at the bottom edge of the iron phototube enclosure. Light from heavier mass particles entered a light collecting cone and was directed to phototube H. Light from lighter particles passed outside of this light collecting cone, were reflected from a spherical mirror at the top of the counter and entered phototube L. The phototubes were isolated from the high pressure gas volume by 1 inch thick quartz windows coated with 54 nm MgF_2. To correct for ambient magnetic fields, each phototube (RCA 31000M) was magnetically shielded and wound with a compensating coil.

4. Velocity Measuring Ĉerenkov Counter, C2

The C2 or 'Flower Power' counter, shown in Fig. 5, was capable of measuring a particle's velocity over a limited range. The pressure vessel body was a steel pipe, internally blackened, and filled with nitrogen as the Ĉerenkov radiating medium. The entrance and exit of the beam from the counter was through 25μm stainless steel windows.

The high sensitivity photomultipliers (RCA 31000Ms) observed the Ĉerenkov light produced in the counter through quartz windows in the pressure vessel. The nitrogen pressure could be varied from 0 to 300 psia to change the observed light ring radius for a given particle velocity.

The Ĉerenkov light was focused to a ring image by the downstream parabolic mirror. The image was produced near the face of the middle mirror, the Flower Mirror. This mirror, illustrated in Fig. 6, was designed to reflect a portion of the light and transmit the rest to the upstream mirror. Light reflecting from the Flower Mirror was collected in the top phototubes (FPC) while the transmitted light went to the bottom phototubes (FPA) via the back mirror. Both phototubes were fitted with compound parabolic cones for optimum light collection[21]. A light ring of larger radius would have a larger proportion of its photons reflected to the upper phototube, FPC, while a smaller ring would go predominantly to the lower phototube, FPA. Thus by comparing the two analog signals a measure of the radius was obtained[22]. Figure 7 shows the angular resolution of the Flower Mirror system. It was obtained by reducing the pressure in C2 until the Ĉerenkov light from pions fell on the Flower Mirror.

Ĉerenkov light rings of radius larger than the outer edge of the Flower Mirror were partially collected by 6 planar mirrors distributd around the Flower Mirror, which reflected the light onto the faces of 6 corresponding phototubes,

FPI1-FPI6. These signals were used to veto low mass particles (mostly pions). For clarity, Fig. 5 shows only one of these six mirrors.

D. Spectrometer Magnet

The spectrometer magnet was 72 in long in the beam direction and had a vertical gap of 10 in and a 24 in width. It gave a momentum resolution, $\Delta p/p$, of approximately 1%. For these measurements, the spectrometer magnet imparted a transverse deflection of $\approx$0.4 GeV/c and operated in a range of magnetic fields which were directly proportional to the current.

III. Experiment Calibration

A. Momentum

In order to determine the particle's momentum, it was necessary to know the magnetic field integral of the spectrometer magnet. This was measured quite accurately by another experiment[23] which used the same magnet and power supply. During that experiment, charged particles with known momenta were tracked through the magnet. The field integral was found to be a linear function of the magnet current in the region used in this experiment. Thus, given the magnetic field value, the momentum of the particles emitted by the channel could be determined.

B. Čerenkov Counters

The radiating gas in C1 was chosen so that a low mass particle would produce approximately 10 photoelectrons at 86.8 GeV/c. The Čerenkov angles in the four other counters was adjusted by controlling the pressure of the nitrogen gas. In

C4 this was to set the Cerenkov threshold while in C2, C3, and C5 it was to match their geometry with the expected particle responses.

Figures 8 and 9 show the number of photoelectrons, N_{pe}, as a function of the gas pressure for several of the counters. For C4 (Fig. 8) the functional dependence of the response is

$$N_{pe} = 2N_0 L\delta P.$$

Here P is the gas pressure, δ is the index of refraction (n) minus one per unit pressure ($\delta P=n-1$), L is the length of the Cerenkov radiating medium, and N_0 is a measure of the counter's efficiency. N_0 is determined to be $\approx 96\ cm^{-1}$.

The response of one of the dual channel counters is shown in Fig. 9. Plotted here is N_{pe} for each of the two channels (H and L) as a function of gas pressure. Note that the position where the two distributions cross gives a useful check of the geometry.

For the Flower Power counter, C2, the response had to be quantified so that the mass of a particle could be determined from its signal. From the mirror shape it was expected that the radius, r, of the Cerenkov light ring is given by

$$r = \tfrac{1}{2}(r_1 + r_2) + \tfrac{1}{\pi}(r_1 - r_2)\sin^{-1}(ASY)$$

where

$$ASY = (g_0 \cdot FPC - FPA)/(g_0 \cdot FPC + FPA)$$

FPA and FPC were the magnitudes of the signals from the phototubes viewing the flower pattern, g_0 was the relative gain of the two light detection systems, and r_1 and r_2 (1.9 and 17.8 cm respectively) were the inner and outer radii of the flower pattern shown in Fig. 6. A detailed study of the angular resolution

curves, such as the one shown in Fig. 8, as a function of gas pressure (hence Čerenkov angle) indicated an anomolous behavior. This behavior could be explained if it was assumed that the Flower Mirror was not concentric with the Čerenkov light ring. An offset of 4.9 cm was sufficient to make all of the data consistent. This offset meant that rings of light which would have fallen off the inside or outside of the Flower Mirror still gave meaningful signals. The ring offset was caused by a misalignment of the imaging mirror and by the beam's passing through the counter slightly off the axis of the mirror. Coulomb scattering of the charged particles, the aberations caused by the mirror's tilt and the chromatic dispersion of the Čerenkov light increased the width of the Čerenkov ring. All these factors contributed to a somewhat degraded resolution and gave rise to a wider angular acceptance of the system. To check these effects, the Flower Mirror system was used to calculate the mass of the antideuteron events. The result, Fig. 10, shows agreement with the known mass within the errors.

IV. Data Acquisition

For most runs, two basic trigger types were used. The first, designated BUPS (Beam UPStream) was simply an indication that a particle had come down the middle of the upstream portion of the apparatus. The second was a BUPS trigger with the added restriction that the trigger particle not have a low mass, called GBLB (Good Beam Low mass Bar). Typically, the BUPS trigger had three basic components. These included a coincidence of three beam defining scintillators and a veto from selected halo scintillators. The third requirement incorporated special logic (called the beam rationer) which allowed events with a second beam particle in temporal proximity to the first to be rejected. This time could be

adjusted so that only one beam particle came within the resolving time of the PWCs.

The GBLB trigger was a BUPS signal with the possibility of a veto from the low mass detecting Čerenkov counters. In most runs, only the vetos from the upstream counters, C1 and FPI1-FPI6, were used in the online trigger.

The two trigger types each went through separate prescalers which were adjusted to produce approximately equal numbers of the two triggers. The prescaled signals were then used to trigger the ADCs, the latches, the PWCs and to start the computer's data acquisition.

The ADCs recorded pulse height information from all of the Čerenkov counters and some of the scintillators. The latches stored the state of all the trigger defining scintillators, all the veto scintillators and the Čerenkov counters. These as well as PWC information were recorded for each trigger.

The experiment used a Digital Equiptment Corporation PDP 11/45 computer, running the Fermilab MULTI program[24], which acquired the data for each event from a CAMAC based data acquisition system. All triggered events were written onto magnetic tape. The computer system performed online diagnostics and analysis as well as some event reconstruction.

The data runs were set up to detect a variety of particles, of assumed charges and masses. This was done by choosing a momentum for the secondary particles to maximize the production cross section, usually at Feynman x = 0 for that particle. Then the Čerenkov counter pressures were set to separate this particle from lower mass ones, in the case of C3, C4, and C5, and to center the expected mass within the acceptance of the measuring range for C2. (See Table I). The rates at which data were actually recorded on tape varied from about 20 per pulse for the particle search runs, to several hundred per pulse for pion runs.

V. Data Reduction

A. Tracking

The tracking procedure was designed to pick out events which passed through the apparatus in a manner consistent with a single particle which did not decay or significantly deviate from a noninteracting trajectory. All events which were on tape had necessarilly passed the BUPS trigger requirement. This already gave a fairly clean beam in the upstream portion of the experiment. The exact path of the particle, as well as its momentum, was determined by the PWCs. Two cuts could be made once the hit positions had been determined. Using the A and B clusters the track could be extrapolated backward to the production target and forward to the D cluster. This extrapolation used the mean momentum for the particles and so was not exact. The first cut required that the forward extrapolated track match the data in the D cluster within 6.5 mm vertically and 9 mm horizontally. If no valid D cluster hits were recorded, no cut was made. The backward extrapolation required the track to intersect the target within 8 mm in the vertical direction. The D cluster cut eliminated events which had momenta substantially different from the mean. Usually these were low momentum particles produced at the end of the channel or in the apparatus, or particles which decayed into lower momentum secondaries.

A least-squares fit, weighted with the PWC measurement errors, was made on the hit coordinates. A 10^{-5} confidence level cut was placed on this fit.

For the antideuteron runs, after the track fitting, a double peak was observed in the momentum spectrum (see Fig. 11). The lower peak was approximately half the momentum of the higher peak and was well below the lowest momentum in the channel emittance. These events were interpreted as the low

momentum tail of the antiprotons coming from the channel. They were produced by interactions in the last part of the channel creating an antiproton which left the channel and entered the experiment instead of being absorbed in the channel's tungsten walls. Another possible source of these antiprotons was from the dissociation of antideuterons. The antiprotons with approximately one half the channel momentum were then selected by the trigger since their velocities were identical to the higher momentum, heavier antideuterons when measured by the trigger Čerenkov counters.

The possibility that this secondary peak was a computational or an instrumental effect was eliminated by looking at the heavy mass search (see Fig. 12) and the pion runs where no such peak was seen. To obtain a pure antideuteron sample, a cut was placed on the momentum distribution to keep only those events with a momentum greater than 25.5 GeV/c. The particle identification efficiency of these runs relative to others was not biased since such a cut had practically no effect. The deuteron and triton runs exhibited a similar problem. However, the tritons were harder to separate from their backgrounds since these included not only protons but also deuterons near the triton momentum.

B. Cuts on Čerenkov Counter Data

The Čerenkov counter signals were used to distinguish low mass from high mass particles. The antideuteron runs were used to determine values for the cuts, since the antideuterons were produced in sufficient quantities to provide a clear signal. Counter, C1, which had been used in the trigger, was not used again in the off-line analysis. The C4 pulse height distribution showed a clean separation between the two peaks where the cut was placed. Figure 13 shows the C4L pulse height versus momentum for an antideuteron run. The one half momentum

antiprotons are clearly visible, trailing into the 'light' particle area as their momentum rises. The previously mentioned momentum cut is also shown. Figure 14 shows a similar plot for a heavy mass search run.

For C3, a scatter plot of C3L versus C3H accentuated the separation, with the cut placed diagonally as indicated. Figure 15 is from an antideuteron run and Fig. 16 is from a heavy mass search run. The C5 data was treated identically. This was justified since the design and operating conditions were the same and experimentally the two counters exhibited similar pulse height distributions. The FP1-FP6 counters in C2 were used only in the on-line analysis. FPC and FPA were not used to reject low mass particles since this might have biased their mass measuring ability. The efficiency of the various counters for identifying antideuterons could then be determined for the given cuts by comparing one to the other two (see Table II). After these cuts, most of the heavy mass candidates lay close to an exact diagonal on the C3 and C5 scatter plots, in particular C3L = C3H and C5L = C5H. This was surprising since antideuteron plots had shown almost no population there.

Sudden changes in the electrical ground level between the experiment and the counting room had been observed. These could explain the spurious signals to the ADCs as well as to the scintillator discriminators which would have had to have produced a trigger. In fact, looking at the scatter plots for C3 and C5 before the tracking cuts, there was a definite enhancement along the diagonal (see Fig. 17). It was observed that these events occurred in both the C3 and C5 counters at the same time. Figure 18 shows a scatter plot of (C5H-C5L) versus (C3H-C3L) under the same conditions as Fig. 17. The diagonal clusterings would project to accumulations of events at zero on each axis. The clustering in the center indicates a strong correlation between the two counters for these events. The spread along C3H-C3L comes from low momentum particles which produce a

signal in C3 and do not get through the spectrometer magnet, therefore producing only pedestals in the C5 ADCs. This indicated that the signals were caused by electrical noise since these counters had in common only the power supplies and some modules in their electronics systems. To remove this background, a tighter cut were placed on C3 and C5 as shown in Fig. 17. This cut was not used for the antideuteron runs. Here the expected number of events where the electrical noise coincided with a real particle track was negligible compared to the antideuterons rate. The efficiency of the counters was therefore somewhat reduced in detecting the high mass particles (see Table III).

VI. Results

A. Antideuterons

A total of $(4.60\pm.07)\ x10^3$ antideuterons passed the analysis cuts. A number of corrections had to be applied to obtain a $\bar{d}/\pi^-$ production ratio. These corrections are ennumerated in Table IV. To get the number of pions observed, N_π, the reconstructed BUPS triggers were examined. They were composed of particles which passed straight through the experimental apparatus satisfying the upstream scintillator trigger and which passed the off line tracking cuts. The approximate composition of this beam was[25] 88% pions, 10% kaons, and ≈2% antiprotons. With the assumption that the PWC tracking was the same for any minimum ionizing charged particle, one gets $\pi^-/BUPS = 0.88$. Thus, for a given run,

$$N_\pi = N_{BUPS} \cdot \frac{\pi}{BUPS} \cdot 2^{(BUPS\ prescale\ factor)}$$

where N_{BUPS} is the number of BUPS triggers, gives the number of reconstructed

pions passing through the apparatus during that run. A total of (1.66±.02) $x10^9$ pions were observed in association with the observed antideuterons.

It was assumed that the PWC tracking efficiency was the same for pions and antideuterons. The relative acceptance of the two particles in the apparatus was also taken to be unity.

The Čerenkov counters were not used in the BUPS determination, so their efficiency was, in effect, 100%. The number of antideuterons was affected by the Čerenkov counters' efficiencies and by the cuts applied to their signals. The efficiency of the three counters which were used to make a positive identification of the antideuterons, C3, C4, and C5, were determined by requiring an antideuteron signal from two of them and counting the fraction of these events which qualified in the third. This was done on an antideuteron run with the actual cuts used. To obtain an overall Čerenkov efficiency it was assumed that the counters' signals were independent of each other. This assumption was not completely true since there was some correlation, but the increased error was small since the individual efficiencies were high. A relative Čerenkov efficiency of 0.945±.015 was used.

To correct for the pion lifetime, one used the fact that in order for a particle to successfully pass the PWC tracking requirement it had to live to reach a distance, z, of 20 m from the target. Assuming a π^- lifetime of $2.60\ x10^{-8}$ sec and a γ of 230, 98.89% survived this distance.

The unequal absorptions of the pions and the antideuterons were accounted for by calculating the amount of each different chemical element in the beam path and obtaining the absorption cross section for pions[26] and antideuterons[13] for these nuclei (see Table V). Summing all these cross sections gave an absorption cross section for the particles passing through the whole apparatus. The results of the fraction surviving were, for the pions 0.8856 ± .0035 and for

the antideuterons 0.6990 ± .0089.

Finally, a correction was made for particle reabsorption in the target. The number of a given particle observed, N^{obs}, for an incident beam flux on the target, B_{inc}, is given by the equation:

$$\frac{N_{\bar{d}}^{obs}}{B_{inc}} = n\sigma_{\bar{d}} \int_0^L e^{-\lambda_p z} \cdot e^{-\lambda_{\bar{d}}(L-z)} \, dz$$

n is the number of nuclei per area in the target, σ is the absorption cross section per nucleus for a given particle, L is the target length, and $1/\lambda$ is the absorption length for a given particle. The $\bar{d}/\pi$ production ratio is given by

$$\frac{\sigma_{\bar{d}}}{\sigma_\pi} = \frac{N_{\bar{d}}^{obs} \, (\lambda_p - \lambda_{\bar{d}}) \cdot (e^{-\lambda_\pi L} - e^{-\lambda_p L})}{N_\pi^{obs} \, (\lambda_p - \lambda_\pi) \cdot (e^{-\lambda_{\bar{d}} L} - e^{-\lambda_p L})}$$

Using,

$$\lambda = 1/\text{absorbtion length} = \frac{\rho N_A \sigma}{A} ,$$

where ρ is the density of the material, N_A is Avogadro's number, A is the atomic number, and σ is the absorption cross sections on copper of 1371, 708, 1270 mb for antideuterons, pions and protons respectively. The value of λ is .117±.006, .052±.003, and .068±.001 cm^{-1} for the three particle types. This gives a relative correction of 1.5865 ± .052 for the run with L = 14.8 cm. Combining all these correction factors

$$\sigma_{\bar{d}} / \sigma_\pi = (5.78 \pm .13) \times 10^{-6}$$

is obtained for protons on copper at the target. A comparison with previously measured values is shown in Fig. 19. It should be noted that a variety of p_t, x_F, and production target material was used in these experiments and are useful

mainly for qualitative comparisons.

B. Heavy Particles

Cuts were applied to the negatively charged high mass search runs which were similar to those used on the negatively charged antideuteron data. After all the cuts had been applied to the high mass search runs, there were no events left which qualified as heavy particles. This fact was used to calculate a limit on the lifetimes and the production cross sections of such particles. Similar to the antideuteron calculations, the number of pions produced during these runs was counted, appropriate corrections made, and a limit obtained.

The corrections are shown in Table VI. Here, as with the antideuterons, the number of pions was obtained from the number of BUPS triggers. The π^- fraction of the beam[25] at this momentum was ≈.9. The measured invariant pion production cross section[27] is 3.19±.16 mb/GeV^2/nucleon. The assumption was made that these heavy particles had the same absorbtion cross section as the pions. Again the Cerenkov counter and PWC efficiencies were calculated similarly to the antideuterons. The lifetime correction for the pions and the heavy particles came from an exponential decay which left 99.6% of the pions and $\exp(-ml/(pc\tau))$ of the heavy particles at the end of the experiment. Here m is the mass, τ the lifetime, p the heavy particle momentum, and l is the length of the experiment. Combining all these factors one gets

$$E\frac{d^3\sigma(m,\tau)}{dp^3} = 3.0 \times 10^{-37} e^{(m/\tau)7.84 \times 10^{-10}} \text{ cm}^2 \text{ GeV}^{-2} \text{ nucleon}^{-1}$$

for a 1 standard deviation limit on the invariant production cross section for heavy negatively charged particles at $p_t = 0$. These limits are shown in Fig. 20.

Particles in the mass range 4 to 6 GeV/c^2 could have been detected and mass

measured by the Flower Power counter. However, charged particles with masses up to the kinematic limit, ≈11 GeV/c^2 (≈12 GeV/c^2 if they were not produced in pairs), could also be detected. The signature of one of these particles would be a normal signal in the beam defining scintillators and the PWCs. Since the particles' velocities would be below the Čerenkov radiating threshold no signal would be seen in any of the Čerenkov counter channels. This event would still pass the GBLB trigger requirements since there would be no Čerenkov signal to indicate a light particle to be vetoed. A limit on the production cross section and lifetime of these particles can be calculated (see Fig. 20) in the same way as was done for the 4 to 6 GeV/c^2 range. In this case, however, the heavy particles are no longer produced near $x_F = 0$ and so their production cross section is expected to be smaller. Although no events of this type were observed, there were a few events which had small values not only for the Čerenkov ADCs, but also for the scintillator ADCs. The mechanism causing such signals is unclear. If these signals were caused by particles traversing the apparatus, they could not be integrally charged. On the other hand, these can be attributed to rare malfunctions of the ADCs.

Most of the high mass search runs were performed in a negative secondary beam, but some runs were in a positively charged beam. This was achieved by simply switching the polarity on all of the magnets while leaving everything else the same. The positively charged data were analyzed in exactly the same way as were the negative runs. After all the cuts, one possible event remained in the 4 to 6 GeV/c^2 range. With only one possible event in the sample, the calculation of the cross section limit for the production of such heavy particles is independent of the validity of the single event. In order to calculate a limit for the production of heavy mass positive particles, some of the correction factors had to be changed because the positive particle

production cross section was measured relative to π^+ rather than the π^-. The fraction[25] of π^+/BUPS was only 0.75 at these energies. By the same procedure and under the same conditions as for the negative particles this gave

$$E\frac{d^3\sigma(m,\tau)}{dp^3} = 1.21 \times 10^{-36} e^{(m/\tau)7.84 \times 10^{-10}} \text{ cm}^2 \text{ GeV}^{-2} \text{ nucleon}^{-1}.$$

The results are shown in Fig. 21.

C. Other Particles

Data was taken to measure the triton production cross section which corresponded to a total incident flux of 2.46×10^9 BUPS. The tritons could not be separated cleanly on the basis of mass. The tails of the much more copiously produced deuterons spread into the triton region. On average, the deuterons had to have 2/3 of the triton's momentum in order to pass the Čerenkov counter trigger cuts. To take advantage of this fact, a scatter plot of momentum versus mass was examined. As shown in Fig. 22, by this method the tritons could be seen, although the separation was still not very clean. The background of the deuterons in the triton region was estimated as a linearly decreasing tail and was subtracted. This left 32±6 tritons in the sample. Using the same method as for the antideuterons, gave a production ratio $t/\pi^+ = (3.56 \pm .70) \times 10^{-8}$. This ratio ignores the difference in their absorption cross sections since no good measurements exist for the triton and the theories give varying values.

Some data were taken to measure the He^3 production cross section. Since He^3 is doubly charged, it needed twice the normal momentum in order to pass through the momentum selecting channel. Similarly the spectrometer magnet and the PWCs measured it as having one-half its actual momentum. The angle of the Čerenkov radiation produced depends on mass/momentum of the particle. Therefore, when a

mass measurement is made with the Flower Power counter, a He^3 nucleus will produce a signal equivalent to a particle of one-half the He^3 mass with the normal channel momentum. This puts the He^3 mass measurement almost exactly one-half way between the proton and the deuteron signals. Both these particles are produced so much more copiously than He^3 that even using the momentum-mass correlation, as with the triton, and requiring a tighter GBLB trigger (C4-veto and B4, B5) the He^3 signal could not be seen above background.

Deuteron measurements were also made. With an analysis analogous to the antideuterons, a d/π^+ production ratio of $(1.10\pm.19)\ x10^{-4}$ was determined. Reference 29 gives more details of this study.

VI. Conclusion

This experiment placed tighter limits than heretofore on the lifetimes and production cross sections in which heavy charged particles could be directly observed. The fact that these particles could have been seen regardless of their decay modes, and to a large extent independent of any of their properties except charge, mass and lifetime, makes this result an important consideration in future theoretical predictions of new particles.

Although they were not the main purpose of the experiment, and therefore not studied in such detail, the data for the light nuclei and antinuclei may, in combination with other experiments, help produce a better understanding of the mechanisms involved in their production.

Acknowledgments

We would like to thank Peter Martin, Ed Steigmeyer, Jack Upton and Mike Catalano for their contributions. We also thank the staff of Fermilab for their help. This work was supported in part by the U. S. Department of Energy under Contract No. DE-AC-02-76-CHO-3000, No. DE-AC-02-76-ERO-3075 and No. W-7405-ENG-82.

References

* Present address: 15 E. 11th St., New York, NY 10003.

† Present address: HEP Division, Argonne National Laboratory. Argonne, IL 60439.

¶ Present address: Enrico Fermi Institute, University of Chicago, Chicago, IL 60637.

†† Present address: Institute of Physics, Warsaw University, Warsaw, Poland.

** Present address: Department of High Energy Physics, University of Helsinki, Helsinki, Finland.

1. L. B. Leipuner et al., Phys. Rev. Lett. 31, 1226 (1973).

2. J. A. Appel et al., Phys. Rev. Lett. 32, 428 (1974).

3. D. Cutts et al., Phys. Rev. Lett. 41, 363 (1978).

4. R. Vidal et al., Phys. Lett. 77B, 344 (1978).

5. H. R. Gustafson et al., Phys. Rev. Lett. 37, 474 (1976).

6. M. Y. Han and Y. Nambu, Phys. Rev. B139, 1006 (1965).

7. J. C. Pati and C. H. Woo, Phys. Rev. D3, 1173 (1971).

8. H. Georgi and S. L. Glashow, Nucl. Phys. B159, 29 (1979).

9. S. Fredriksson and M. Jaendel, Phys. Rev. Lett. 48, 14 (1982).

10. A. Filone, Nuovo Cimento Suppl. 12, 353(1954); E. M. Friedlander, et al., Phys. Rev. Lett. 45, 1084(1980).

11. I. Hinchliffe and L. Littenberg, LBL 15022, 1982 (unpublished).

12. M. Chanowitz and S. Sharpe, LBL 15749, 1983 (unpublished).

13. L. W. Jones et al., Phys. Rev. 164, 1584 (1967).

14. J. A. Goodman et al., Phys. Rev. D19, 2572 (1979).

15. S. P. Denisov et al., Nucl. Phys. B31, 253 (1971).

16. D. Cutts et al., in Proceedings of the IV International Antiproton Symposium, Strasbourg, France (1978).

17. W. Bozzoli et al., Nucl. Phys. B144, 317 (1978).

18. T. R. Cardello, Ph.D. thesis, Yale University, 1983.

19. P. A. Souder, J. Sandweiss and A. A. Disco, Nucl. Instrum. Methods 109, 237 (1973).

20. C. R. Kerns, Fermilab TM-650, 2100.00, 1976 (unpublished).

21. H. Hinterberger and R. Winston, Rev. Sci. Instrum. 37, 1094 (1966); R. Winston, J. Opt. Soc. Am. 60, 245 (1970).

22. V. L. Fitch, "A Broad-Band Focusing Cherenkov Counter", Princeton University Technical Report (unpublished); R. Cester et al., IEEE Trans. Nucl. Sci. NS-25 No. 1, 525 (1978).

23. Y. W. Wah, Ph.D. thesis, Yale University, 1983.

24. J. F. Bartlett et al., Fermilab PN-97.4, 1978 (unpublished).

25. K. Doroba, Fermilab TM-818, 1978 (unpublished).

26. A. S. Carroll et al., Phys. Lett. 80B, 319 (1979).

27. F. E. Taylor et al., Phys. Rev. D14, 1217 (1976).

28. M. G. Albrow et al., Nucl. Phys. B97, 189 (1975); B. Alper et al., Phys. Lett. 40B, 265 (1973); Yu. M. Antipov et al., Phys. Lett. 34B,164 (1971); T. Binon et al., Phys. Lett. 30B, 506 (1969); D. Cutts et al., Phys. Rev. Lett. 41, 403 (1978); D. E. Dorfan et al., Phys. Rev. Lett. 14, 995 (1965); FSAS Group, Fermilab Report, NAL-73/83-EXP (unpublished); References 2 and 17; J. Nassalski and I. Zielinski, "A Study of the Production of Light Antinuclei ($\bar{p}$, $\bar{d}$) in Nuclear Interactions" Fermilab Letter of Intent, 1979 (unpublished).

29. J. L. Thron, Ph.D. Thesis, Yale University, 1983.

PARTICLE TYPE	PION FLUX	MOMENTUM (GeV/c)
NEGATIVE HEAVY MASS	3.0×10^{10}	86.8
POSITIVE HEAVY MASS	0.6×10^{10}	86.8
ANTIDEUTERONS	2.9×10^{9}	31.2
DEUTERONS	7.0×10^{8}	31.2
TRITONS	2.5×10^{9}	47.6
He^3	1.6×10^{9}	27.8

TABLE I Types of data runs, showing the total pion flux through the experiment for that type of run. Also shown is the secondary momentum chosen for the study. In all cases the primary beam was at 400 GeV/c.

COUNTER	EFFICIENCY
C3	100.0±0.5%
C4	96.8±1.1%
C5	97.6±1.0%
TOTAL	94.5±1.5%

TABLE II The efficiency of the Cerenkov counters for correctly identifying an antideuteron with the cuts as described for the antideuteron runs.

COUNTER	EFFICIENCY
C3	98.6±0.9%
C4	97.6±1.1%
C5	87.7±2.3%
TOTAL	84.4±2.5%

TABLE III The efficiency of the Cerenkov counters for correctly identifying a high mass particle with the cuts as decribed for those runs.

DESCRIPTION	CORRECTION
$\frac{\text{NONDECAYED } \pi^-}{\text{NONDECAYED } \bar{d}}$	.95±.01
RELATIVE ABSORPTION IN APPARATUS ($\bar{d}/\pi$)	1.27±.01
RELATIVE REABSORPTION IN TARGET ($\bar{d}/\pi$)	1.54±.05
RELATIVE CERENKOV EFFICIENCIES ($\bar{d}/\pi$)	.945±.015
RELATIVE PWC TRACKING EFFICIENCY	1.0

TABLE IV Corrections applied to the observed antideuteron to beam ratio to obtain an antideuteron to pion production cross section ratio.

NUCLEUS	ATM. NO.	$\rho L (\times 10^{22})$ (NUCLEI/c^2)	$\sigma_{\bar{d}} \rho L$	$\sigma_{\pi} \rho L$
H	1	9.14	0.0107±0.0006	0.0024±0.0001
C	12	9.03	0.0483±0.0025	0.0155±0.0007
N	14	41.42	0.238 ±0.012	0.0800±0.0037
O	16	1.96	0.0121±0.0006	0.0042±0.0002
F	19	.74	0.0051±0.0003	0.0018±0.0001
Al	27	.84	0.0071±0.0004	0.0027±0.0002
Si	28	.57	0.0051±0.0003	0.0019±0.0001
Cl	35	.37	0.0036±0.0002	0.0014±0.0001
Ar	40	.24	0.0027±0.0002	0.0010±0.0001
Fe	56	1.90	0.0256±0.0013	0.0105±0.0006
TOTAL			0.358 ±0.013	0.121 ±0.004

TABLE V List of material traversed by the beam in the apparatus and the number of total absorbtion lengths ($\sigma\rho L$) for anti-deuterons and pions due to this material.

DESCRIPTION	CORRECTION
$\frac{\text{NUMBER OF MASSIVE PARTICLES}}{\text{NUMBER OF } \pi^-}$	$\frac{1\pm1}{(1.21\pm.02)\times10^{10}}$
$\frac{\text{NONDECAYED } \pi^-}{\text{NONDECAYED MASSIVE PARTICLE}}$	$\frac{.996\pm.001}{\text{EXP}((-m/(\tau\times7.84\times10^{-10}))}$
RELATIVE ABSORPTION IN APPARATUS	1
RELATIVE REABSORPTION IN TARGET	1
RELATIVE CERENKOV EFFICIENCIES (MASSIVE/π)	$.844\pm.025$
RELATIVE PWC TRACKING EFFICIENCY	1

TABLE VI Corrections applied to the heavy mass search observations to obtain a production cross section limit (1σ).

FIGURE CAPTIONS

FIG. 1. Momentum selecting channel. (Not to scale.) The non-interacting beam is dumped in the enlarged upstream section of the channel.

FIG. 2. A side view of the experimental equipment. Shown are the hyperon magnet and channel, the spectrometer magnet, the trigger scintillation Counters (Bi), the Čerenkov counters (Ci) and the PWC clusters.

FIG. 3. Threshold Cerenkov counter, C4, for vetoing fast particles. The primary mirror is the 45° planar mirror on the right. The spherical mirror on the top right focused the Čerenkov light onto the RCA 31000M photomultiplier mounted in the housing in the lower right of the diagram.

FIG. 4. Dual channel Cerenkov counters, C3 and C5. The primary (spherical) mirror focused the Čerenkov light for heavy mass particles, after reflection from the 45° planar mirror, into the lower light collecting cone. Light from lower mass particles was collected by the spherical mirror on the upper left of the diagram and focused into the upper light collecting cone.

FIG. 5. Flower Power Cerenkov counter, C2, for measuring the velocities of the particles. The primary (parabolic) mirror, on the right, focused the Čerenkov light onto the Flower Mirror. The light intercepted by that mirror was collected in the FPC channel. That which was not intercepted by the Flower Mirrow was collected by the FPA photomultiplier after reflection from the sperical mirror on the left. Light from low mass particles was sampled by small 2"x2" mirrors mounted at 45° and reflected onto the six photomultipliers FP1 through FP6.

FIG. 6. The Flower mirror in C2; the white areas are reflecting, aluminized sections of a parabolic mirror, while the black regions are cut away to allow light to pass through.

FIG. 7. Angular resolution of the flower mirror system. Here σ is the standard deviation.

FIG. 8. C4 response curve.

FIG. 9. C3 response curve in the region of the high and low mass channel crossover. The expected overlap range of 3 mrad is indicated.

FIG. 10. Antideuteron mass as computed from C2.

FIG. 11. Momentum distribution of an antideuteron run, showing the cut used to reject the antiprotons.

FIG. 12. Momentum distribution for a heavy particle search run.

FIG. 13. C4 pulse height versus momentum for an antideuteron run, showing the C4 pulse height cut to reject fast particles and the momentum cut to reject antiprotons.

FIG. 14. C4 pulse height versus momentum for a heavy particle search run, showing the C4 pulse height cut to reject low mass particles.

FIG. 15. C3H versus C3L for an antideuteron run showing the clean separation of the antideuterons from the faster particles and the cut applied to reject the latter.

FIG. 16. C3H versus C3L for a heavy particle search run showing the cut to reject the low mass particles.

FIG. 17. C3H versus C3L for an antideuteron run with no PWC tracking required, showing the diagonal band of electronic noise and the cut used to reject it.

FIG. 18. C5H-C5L versus C3H-C3L for an antideuteron run, showing the strong correlation between the two independent counters of the electronic noise.

FIG. 19. Compilation of some antideuteron production cross section experiments. The line shows the production for antiprotons at half the antideuteron momentum, squared, as a model for the antideuteron. A similar plot originally came from the last entry in reference 28.

FIG. 20. New limits set for heavy particle production. Regions to the upper right of the curves are excluded. Cutts, et al. and Vidal, et al. are data from References 3 and 4 respectively.

FIG. 21. New limit set for heavy positively charged particle production. The curve is for a 6 GeV/c^2 particle.

FIG. 22. Momentum versus mass for a triton run showing the triton-deuteron separation.

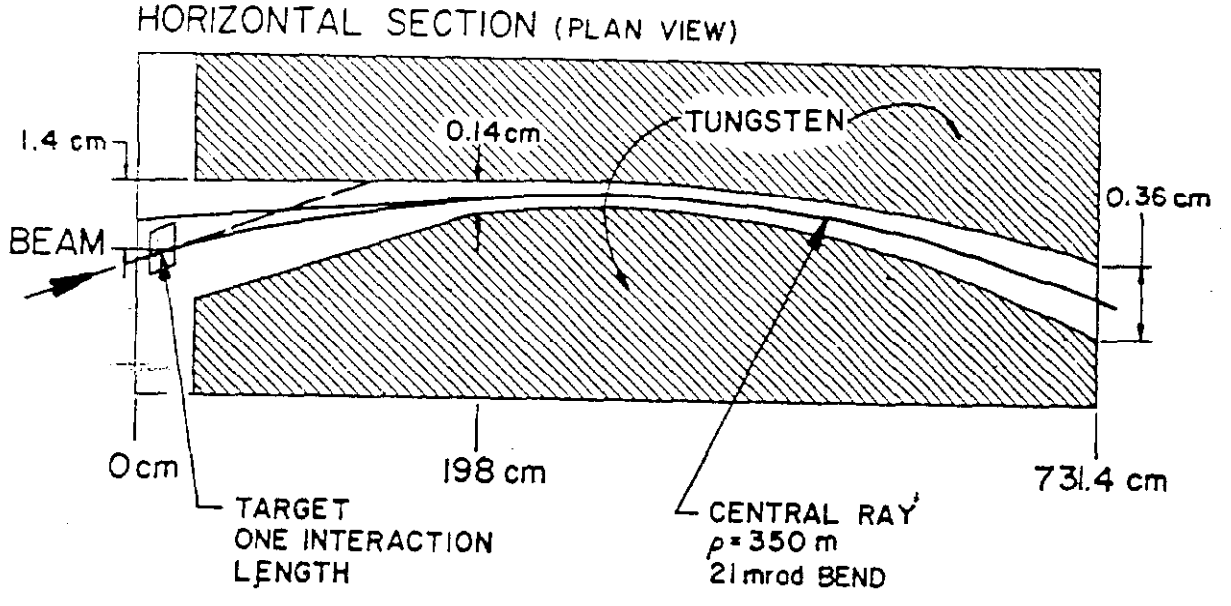
HORIZONTAL SECTION (PLAN VIEW)
1.4 cm
0.14 cm
TUNGSTEN
0.36 cm
BEAM
0 cm
198 cm
731.4 cm
TARGET
ONE INTERACTION
LENGTH
CENTRAL RAY
ρ = 350 m
21 mrad BEND

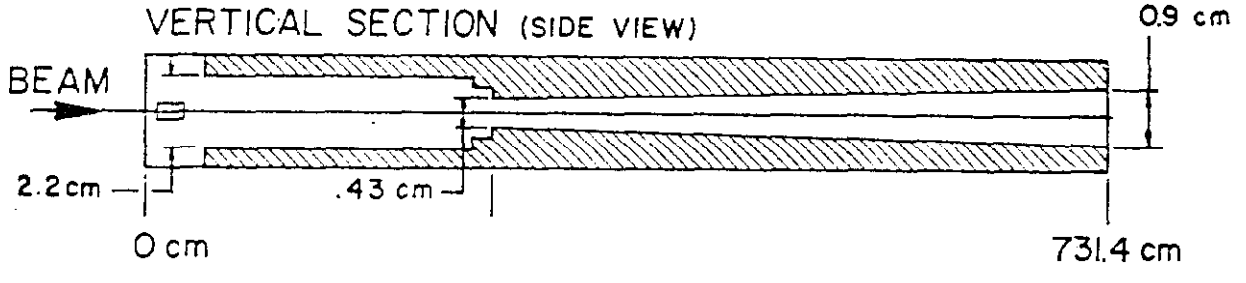
VERTICAL SECTION (SIDE VIEW)
0.9 cm
BEAM
2.2 cm
.43 cm
0 cm
731.4 cm

Fig. 1

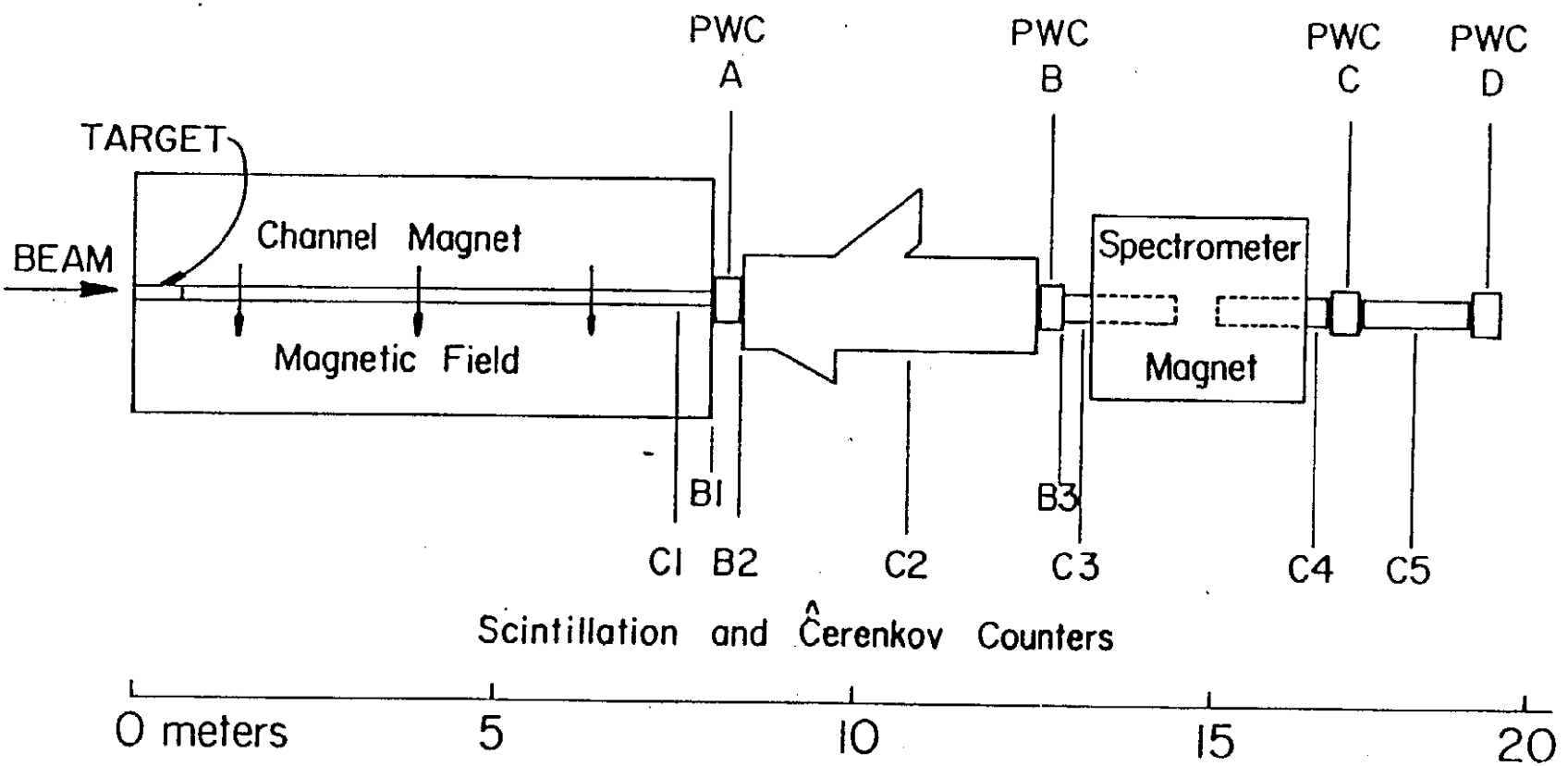
PWC
A
PWC
B
PWC
C
PWC
D
TARGET
BEAM
Channel Magnet
Magnetic Field
Spectrometer
Magnet
B1
B3
C1
B2
C2
C3
C4
C5
Scintillation and Čerenkov Counters
0 meters
5
10
15
20

Fig. 2

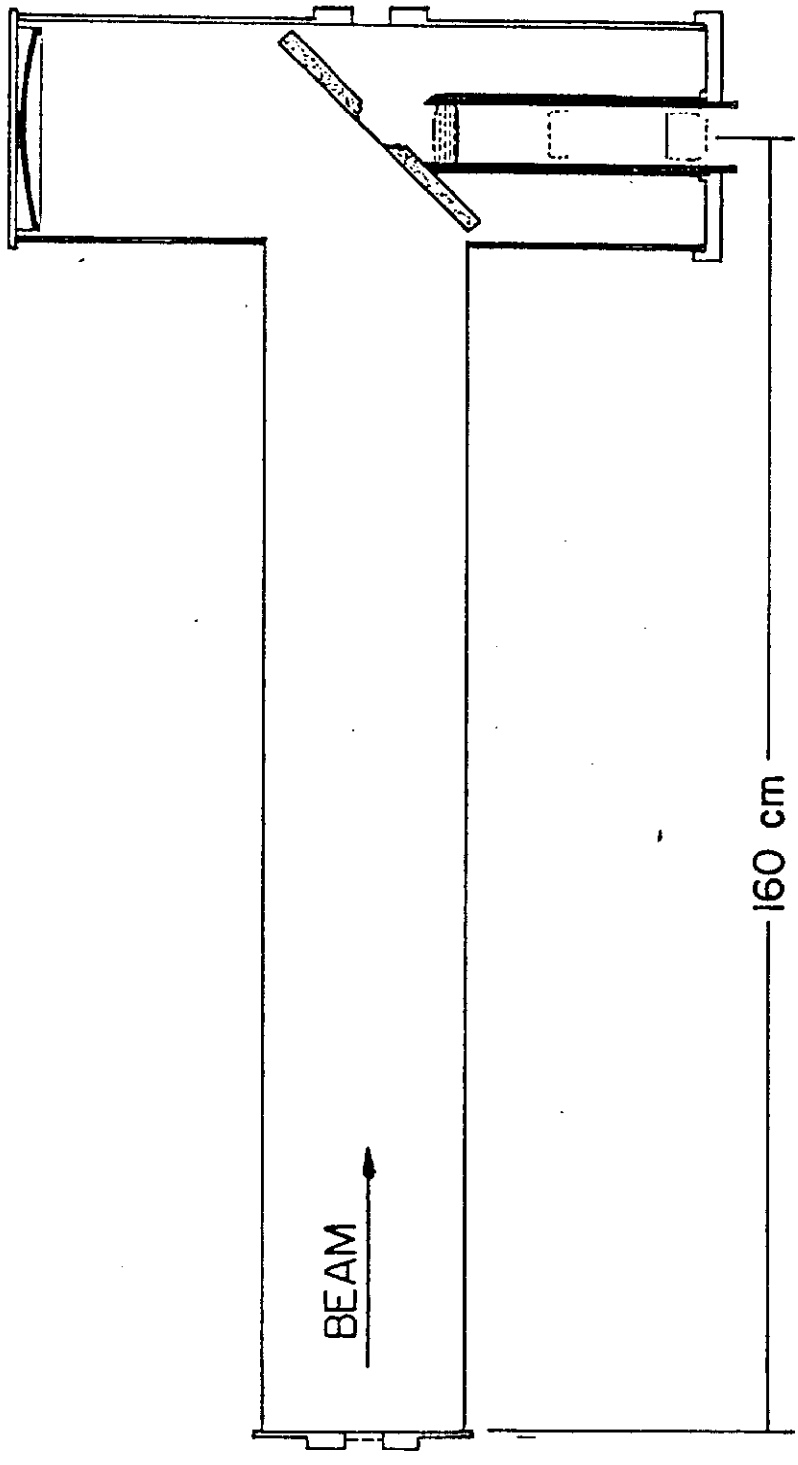

Fig. 3

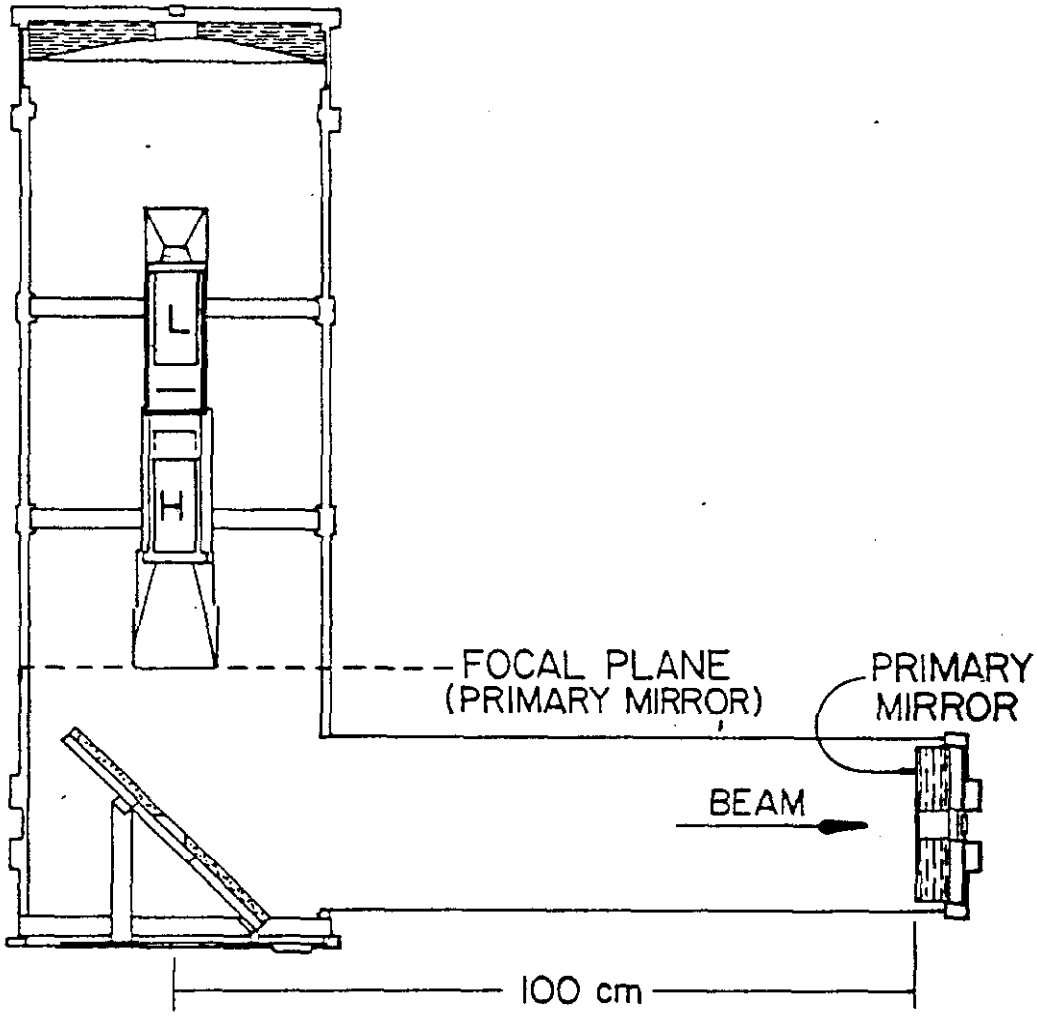

Fig. 4

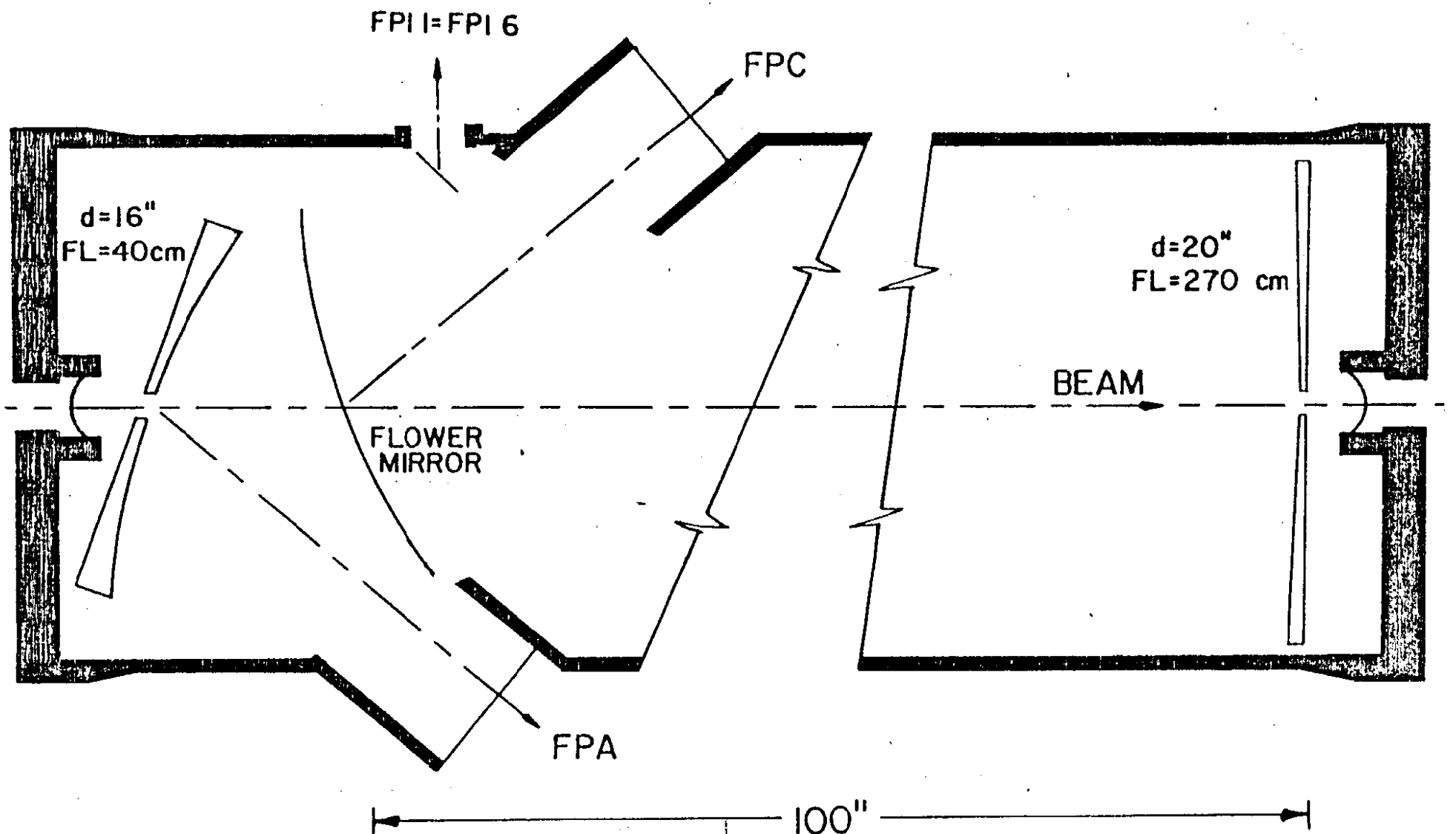
FP11=FP16
FPC
d=16"
FL=40cm
d=20"
FL=270 cm
BEAM
FLOWER
MIRROR
FPA
100"

Fig. 5

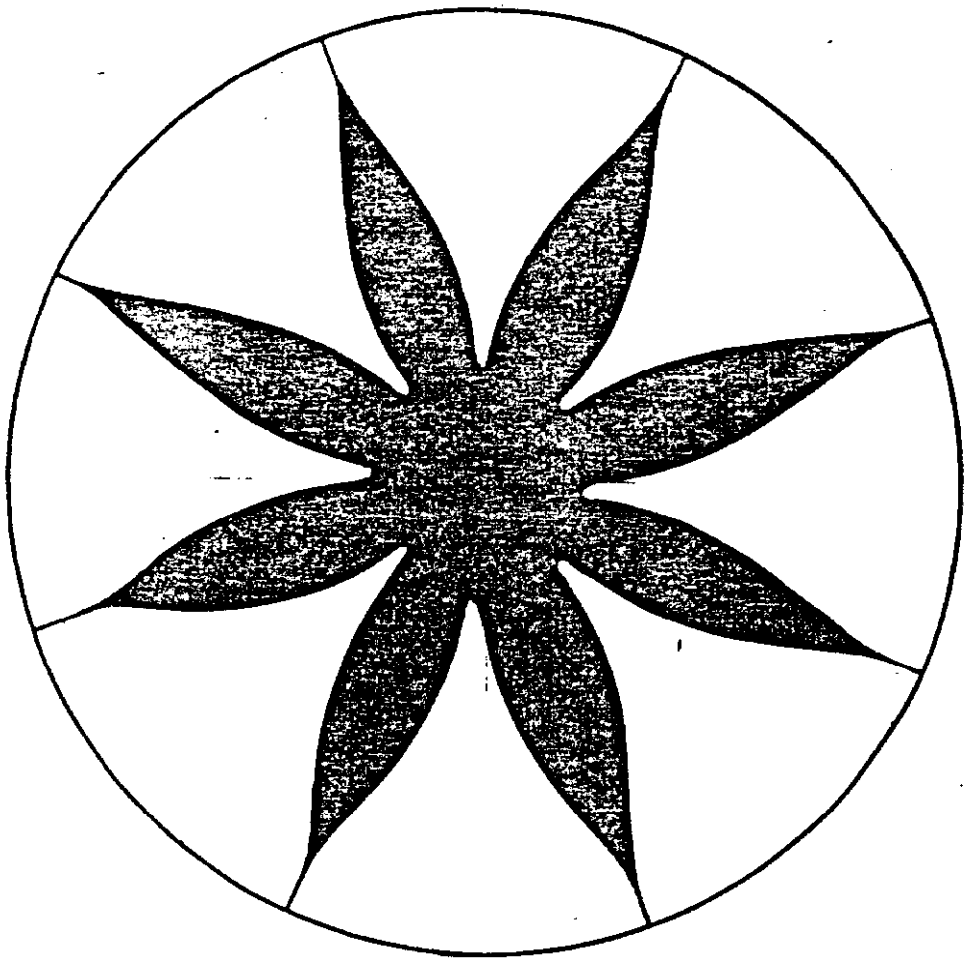

Fig. 6

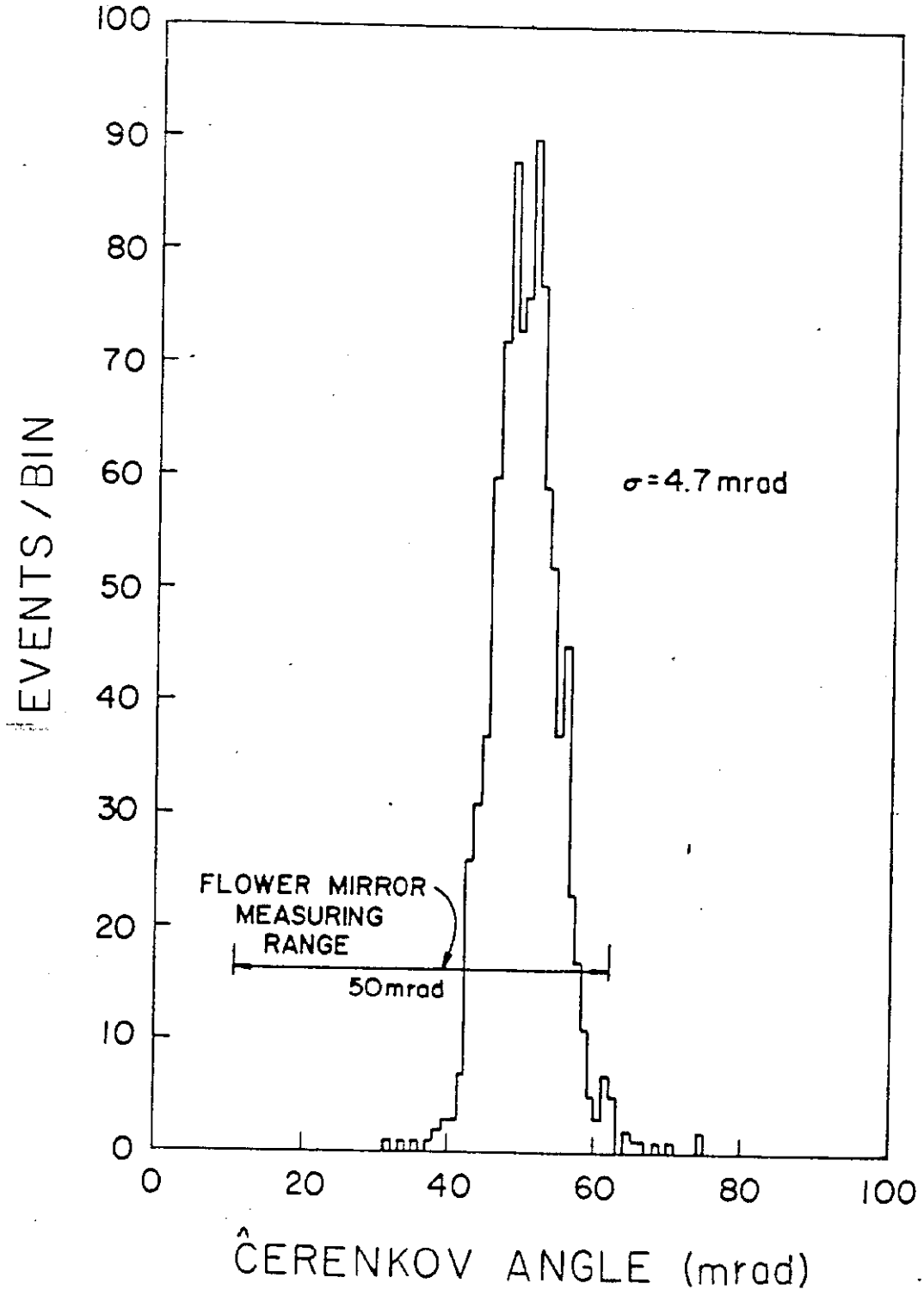
100
90
80
70
60
50
40
30
20
10
0
EVENTS / BIN
σ=4.7 mrad
FLOWER MIRROR
MEASURING
RANGE
50mrad
0
20
40
60
80
100
ĈERENKOV ANGLE (mrad)

Fig. 7

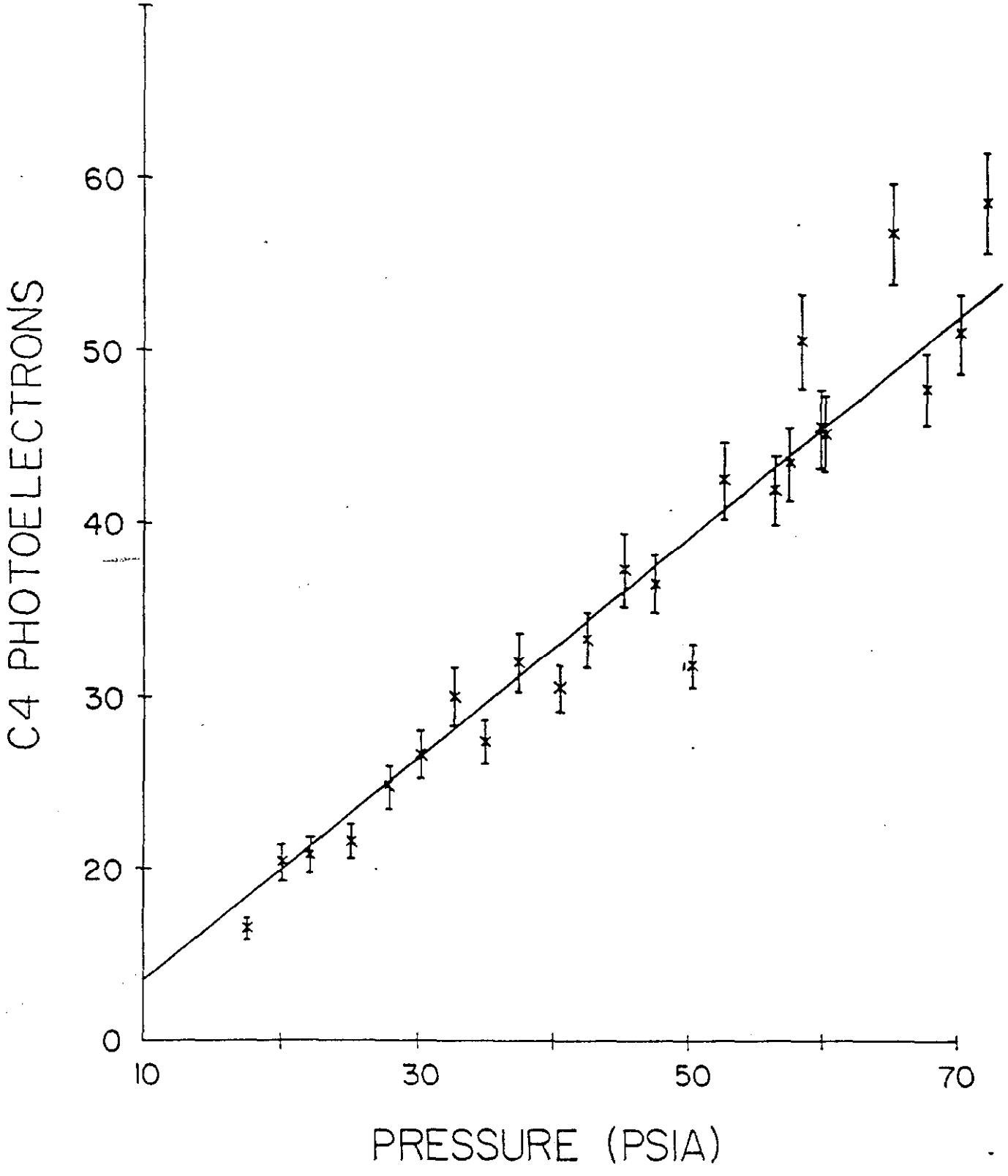

Fig. 8

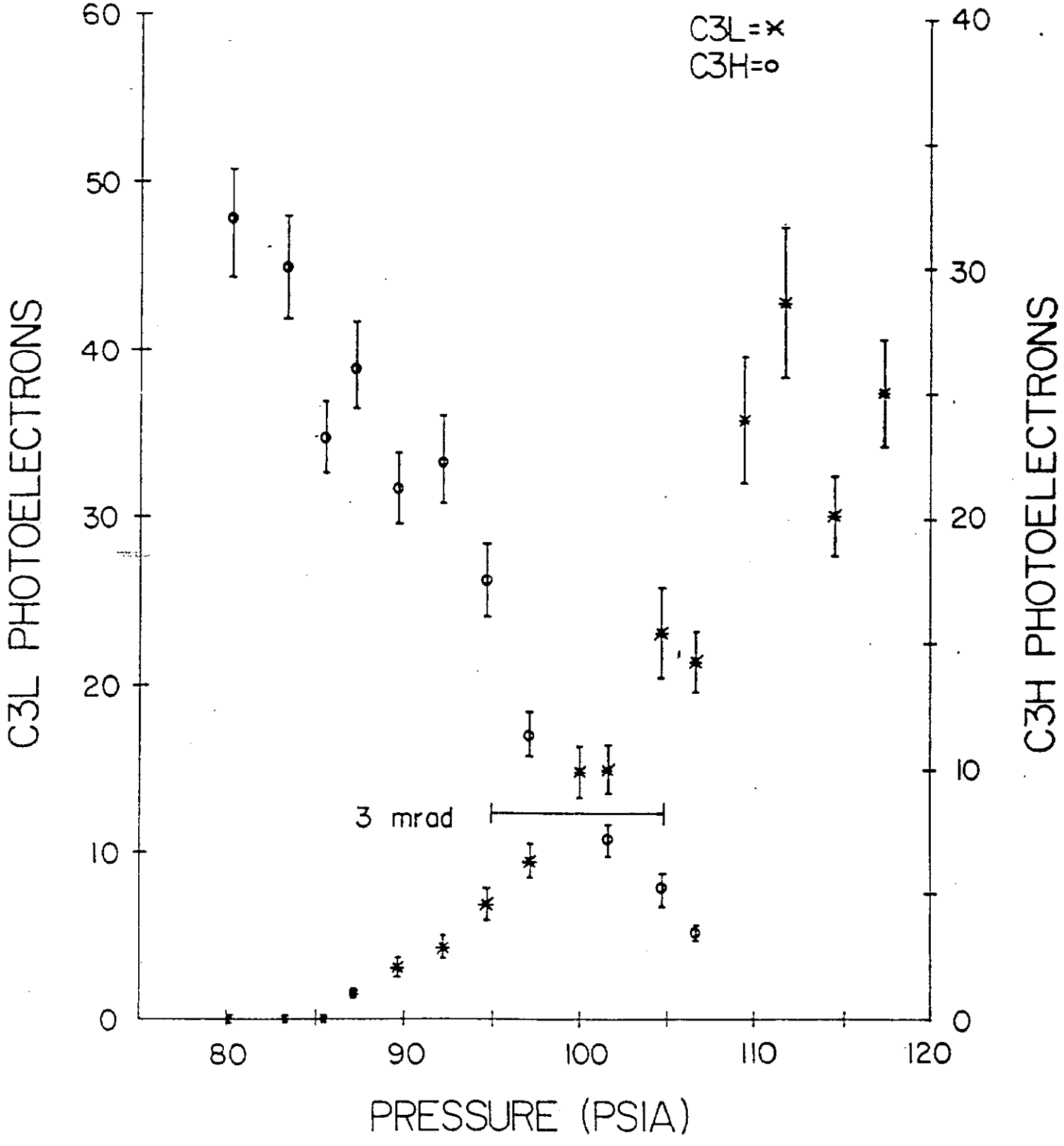
C3L=×
C3H=o
C3L PHOTOELECTRONS
C3H PHOTOELECTRONS
PRESSURE (PSIA)
3 mrad
60
50
40
30
20
10
0
40
30
20
10
0
80
90
100
110
120

Fig. 9

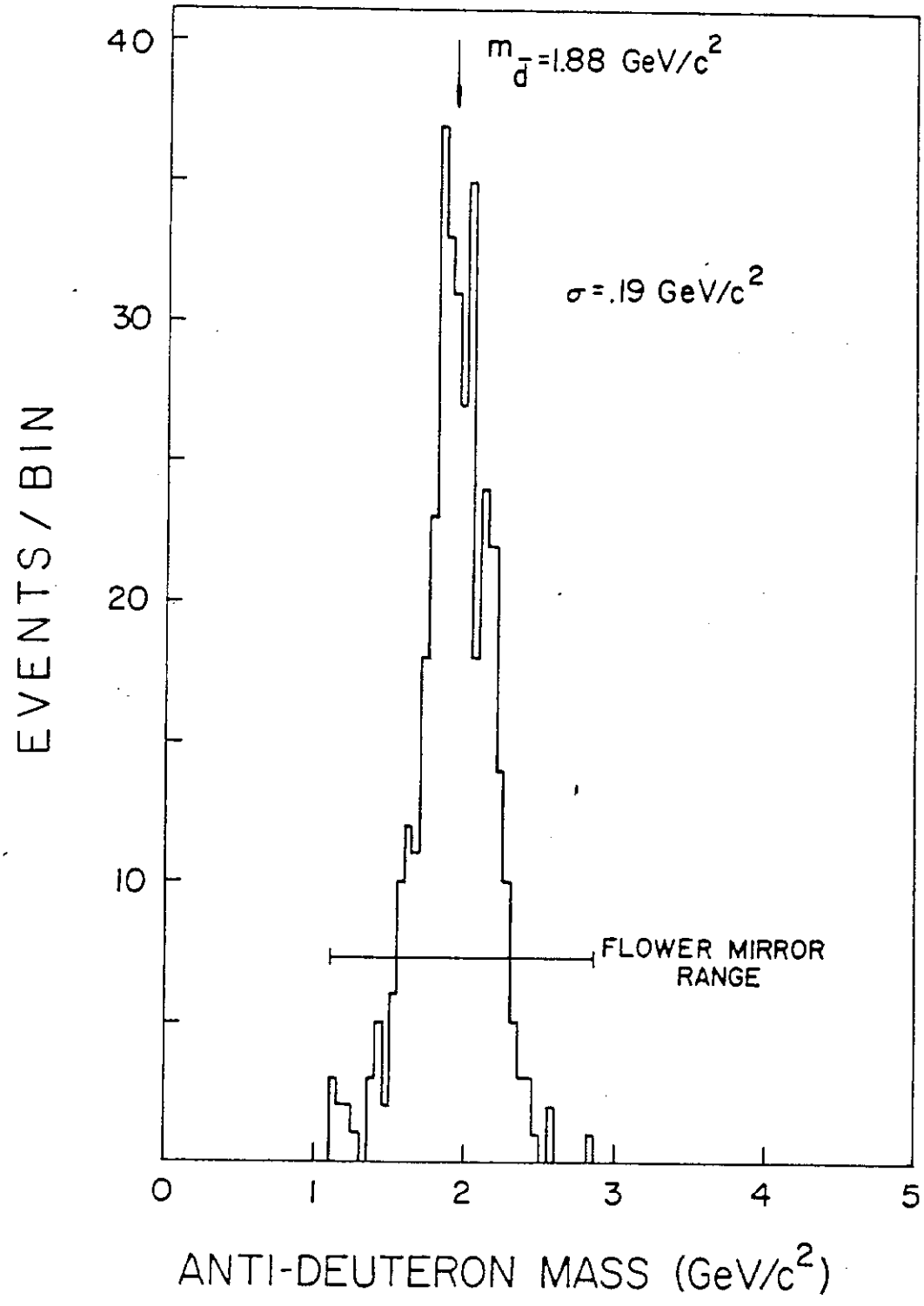
40
30
20
10
0
1
2
3
4
5
EVENTS / BIN
$m_{\bar{d}}$ = 1.88 GeV/c^2
σ = .19 GeV/c^2
FLOWER MIRROR RANGE
ANTI-DEUTERON MASS (GeV/c^2)

Fig. 10

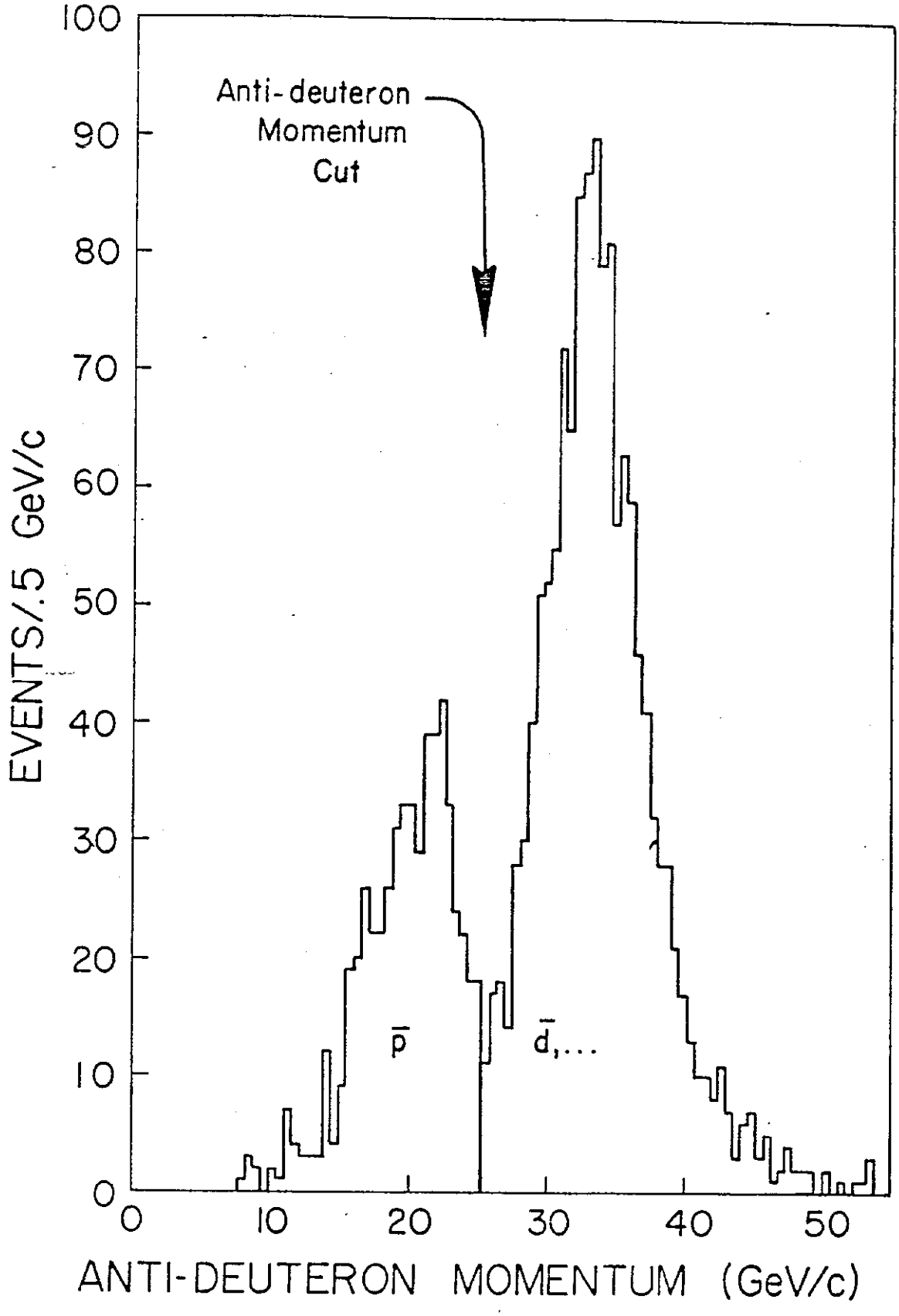
Anti-deuteron
Momentum
Cut
$\bar{p}$
$\bar{d}$,...
EVENTS/.5 GeV/c
ANTI-DEUTERON MOMENTUM (GeV/c)
0
10
20
30
40
50
60
70
80
90
100

Fig. 11

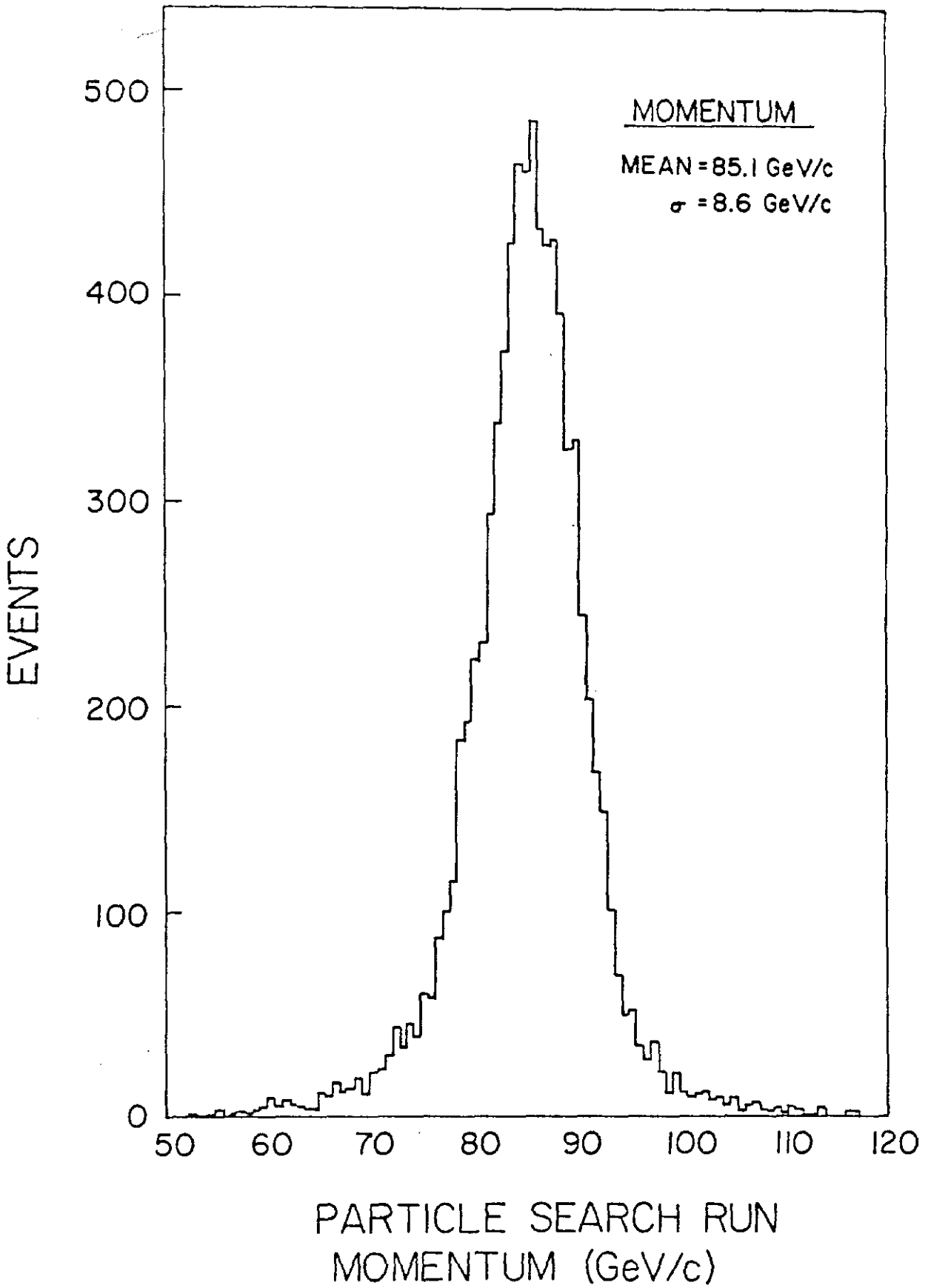
MOMENTUM
MEAN = 85.1 GeV/c
σ = 8.6 GeV/c
EVENTS
0
100
200
300
400
500
50
60
70
80
90
100
110
120
PARTICLE SEARCH RUN
MOMENTUM (GeV/c)

Fig. 12

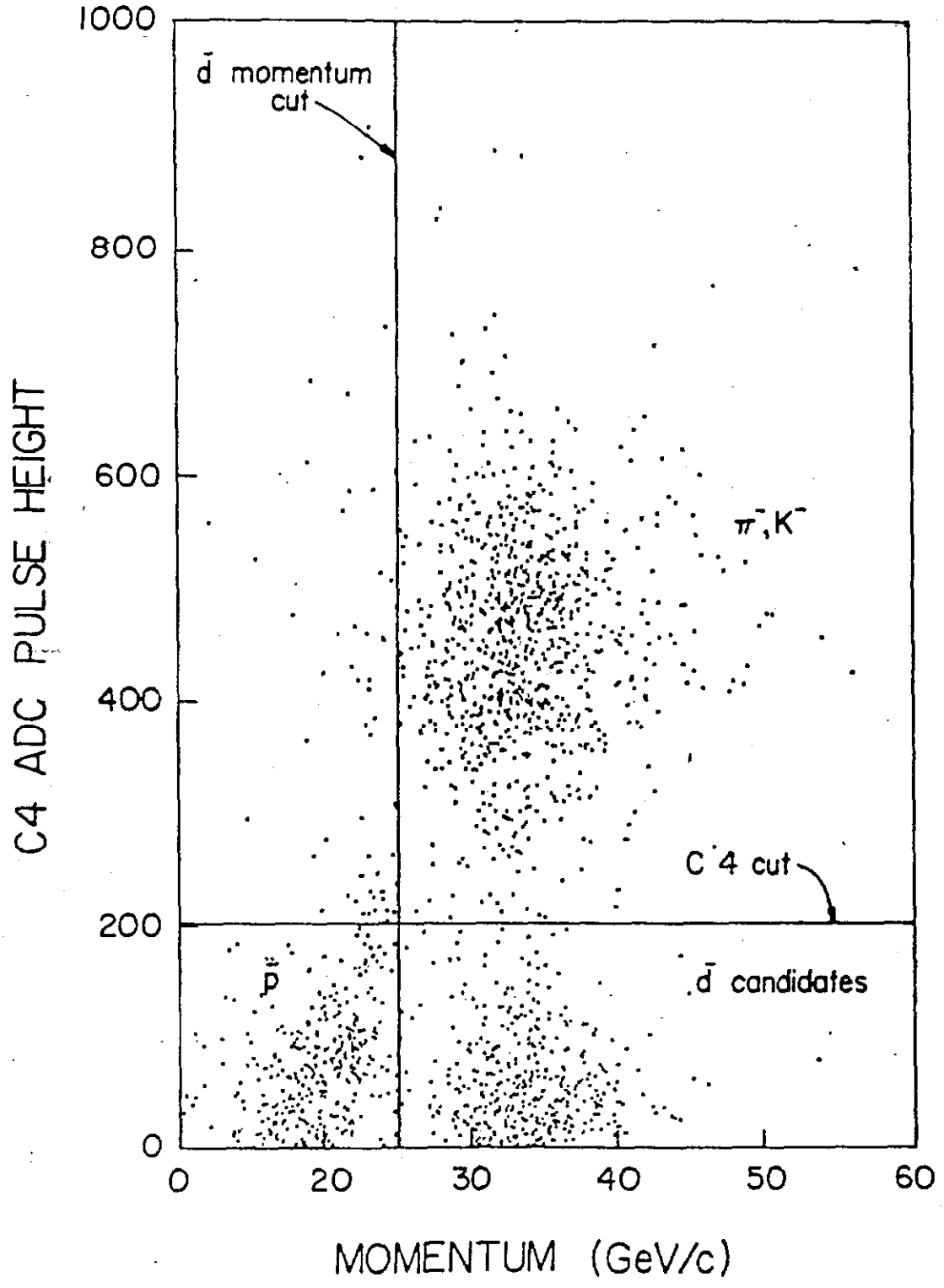
1000
800
600
400
200
0
C4 ADC PULSE HEIGHT
d̄ momentum cut
π⁻, K⁻
C 4 cut
p̄
d̄ candidates
0
20
30
40
50
60
MOMENTUM (GeV/c)

Fig. 13

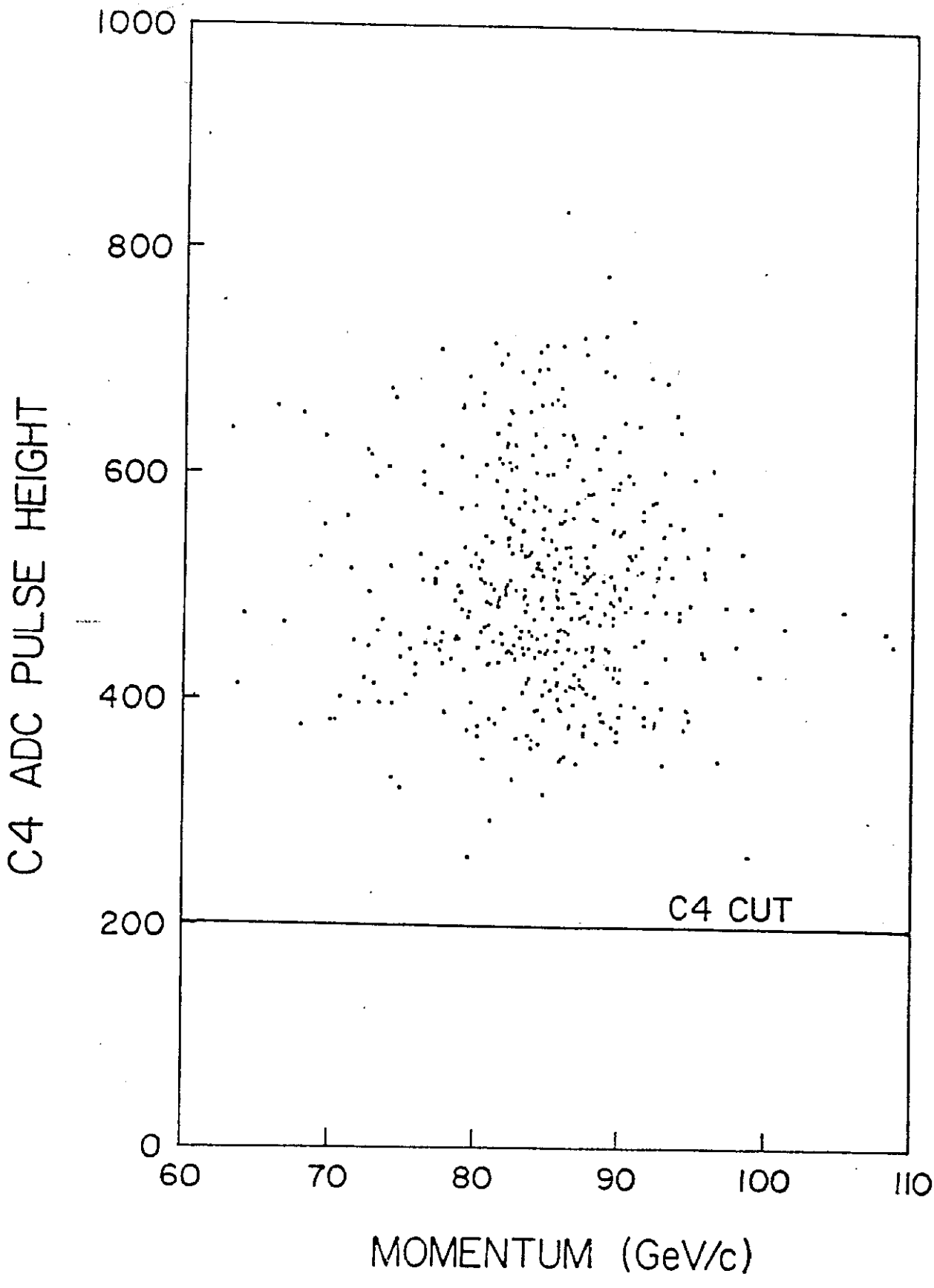
1000
800
600
400
200
0
C4 ADC PULSE HEIGHT
C4 CUT
60
70
80
90
100
110
MOMENTUM (GeV/c)

Fig. 14

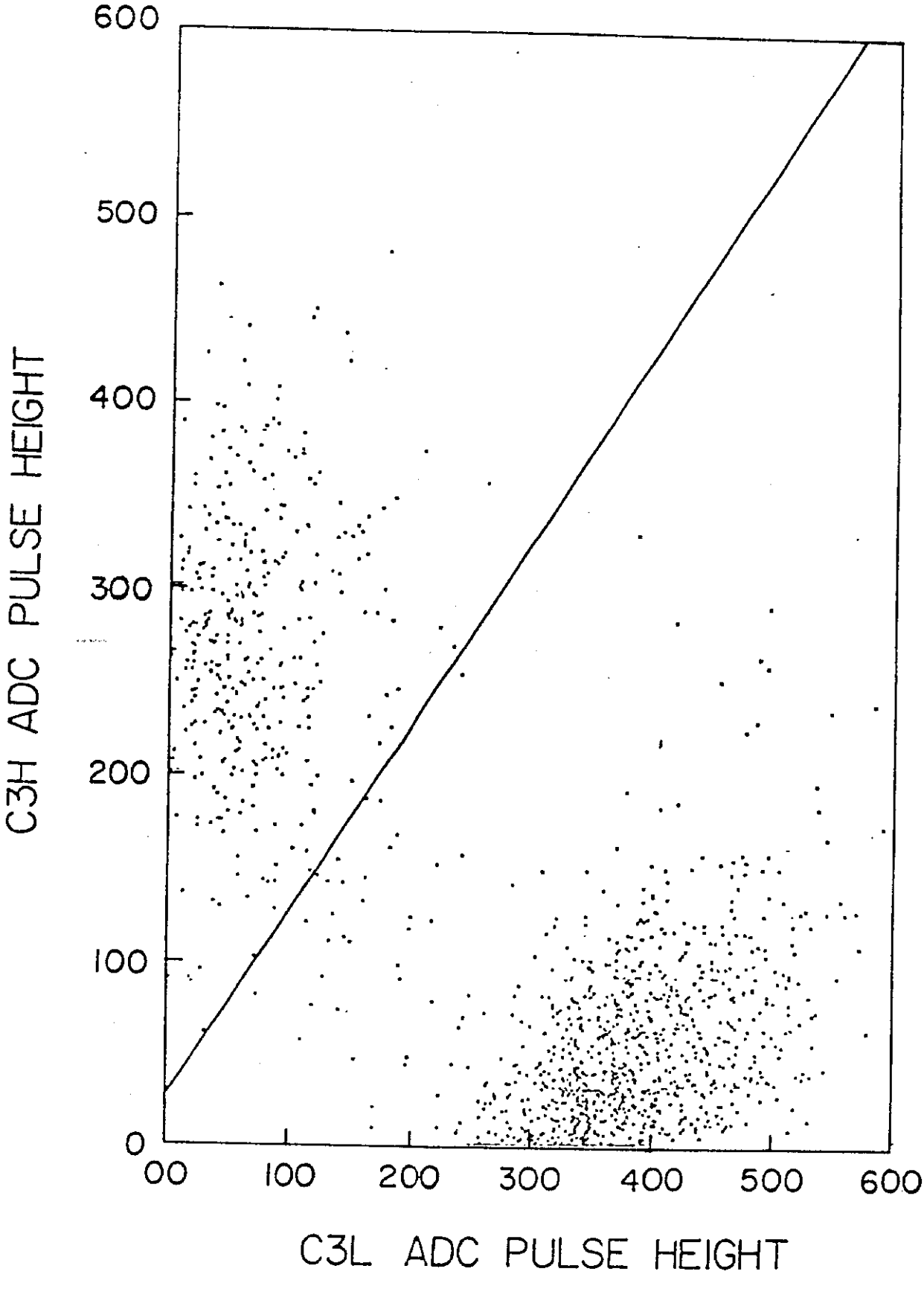
600
500
400
300
200
100
0
00
100
200
300
400
500
600
C3H ADC PULSE HEIGHT
C3L ADC PULSE HEIGHT

Fig. 15

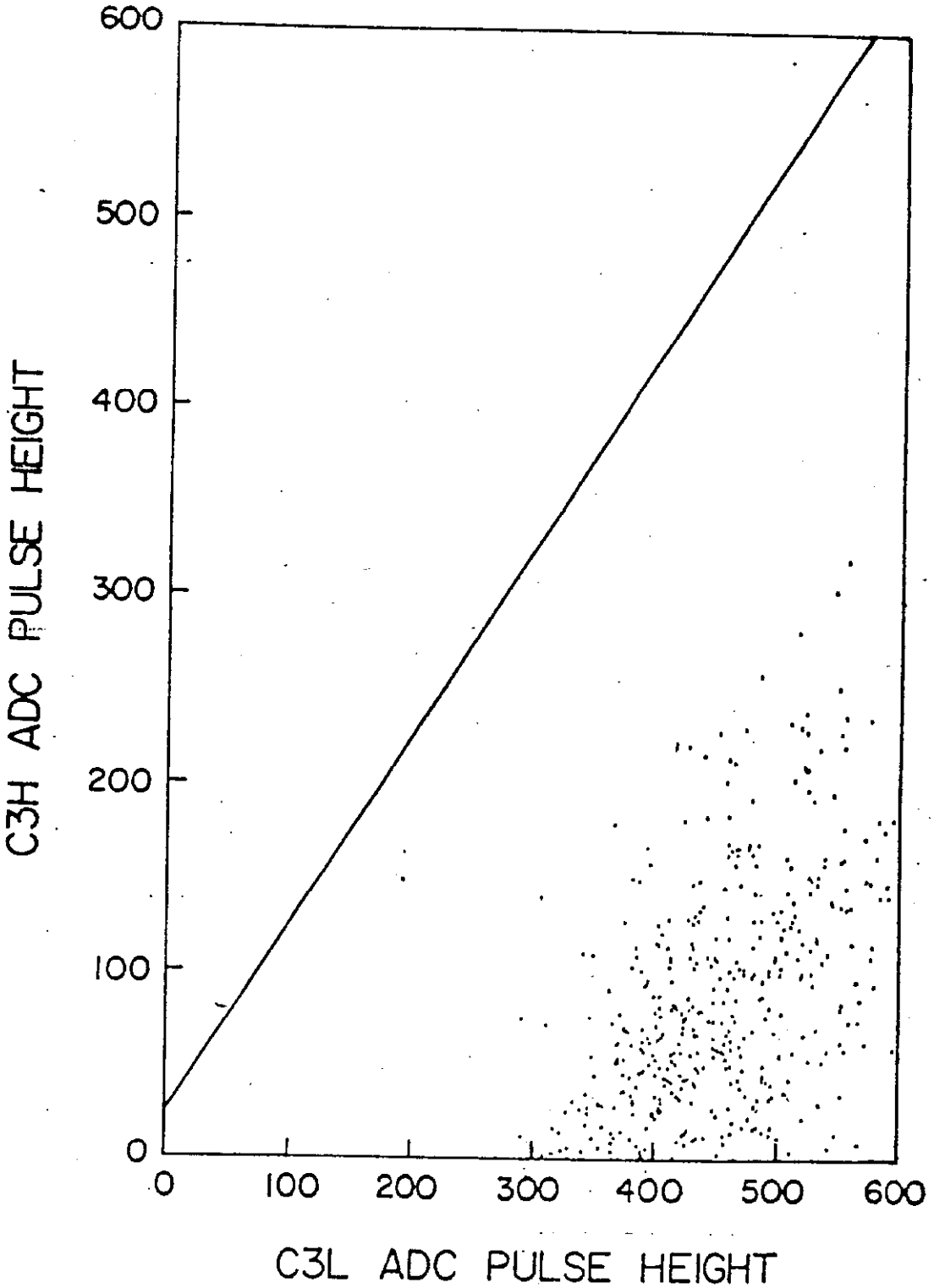
600
500
400
300
200
100
0
C3H ADC PULSE HEIGHT
0
100
200
300
400
500
600
C3L ADC PULSE HEIGHT

Fig. 16

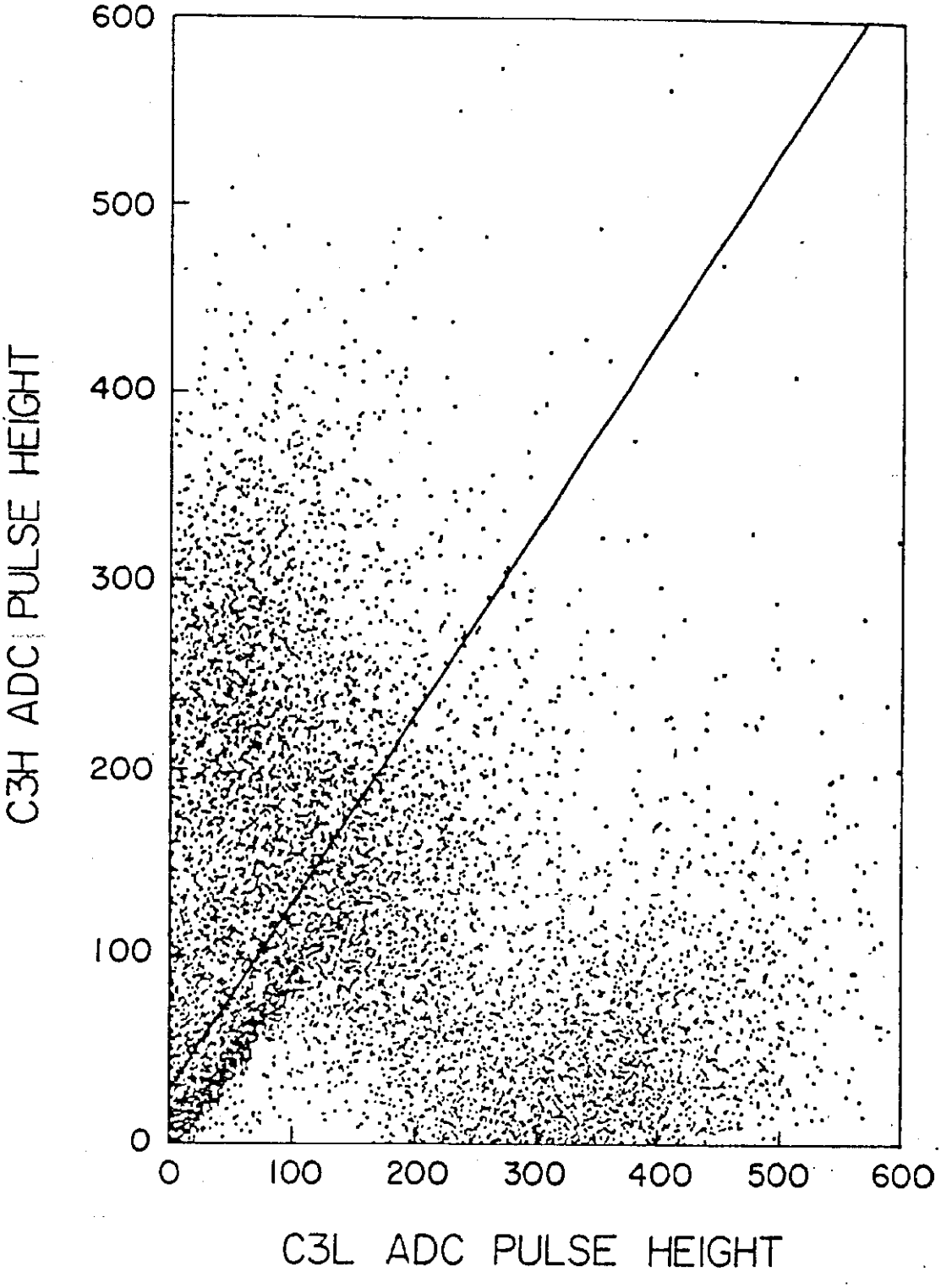
600
500
400
300
200
100
0
C3H ADC PULSE HEIGHT
0
100
200
300
400
500
600
C3L ADC PULSE HEIGHT

Fig. 17

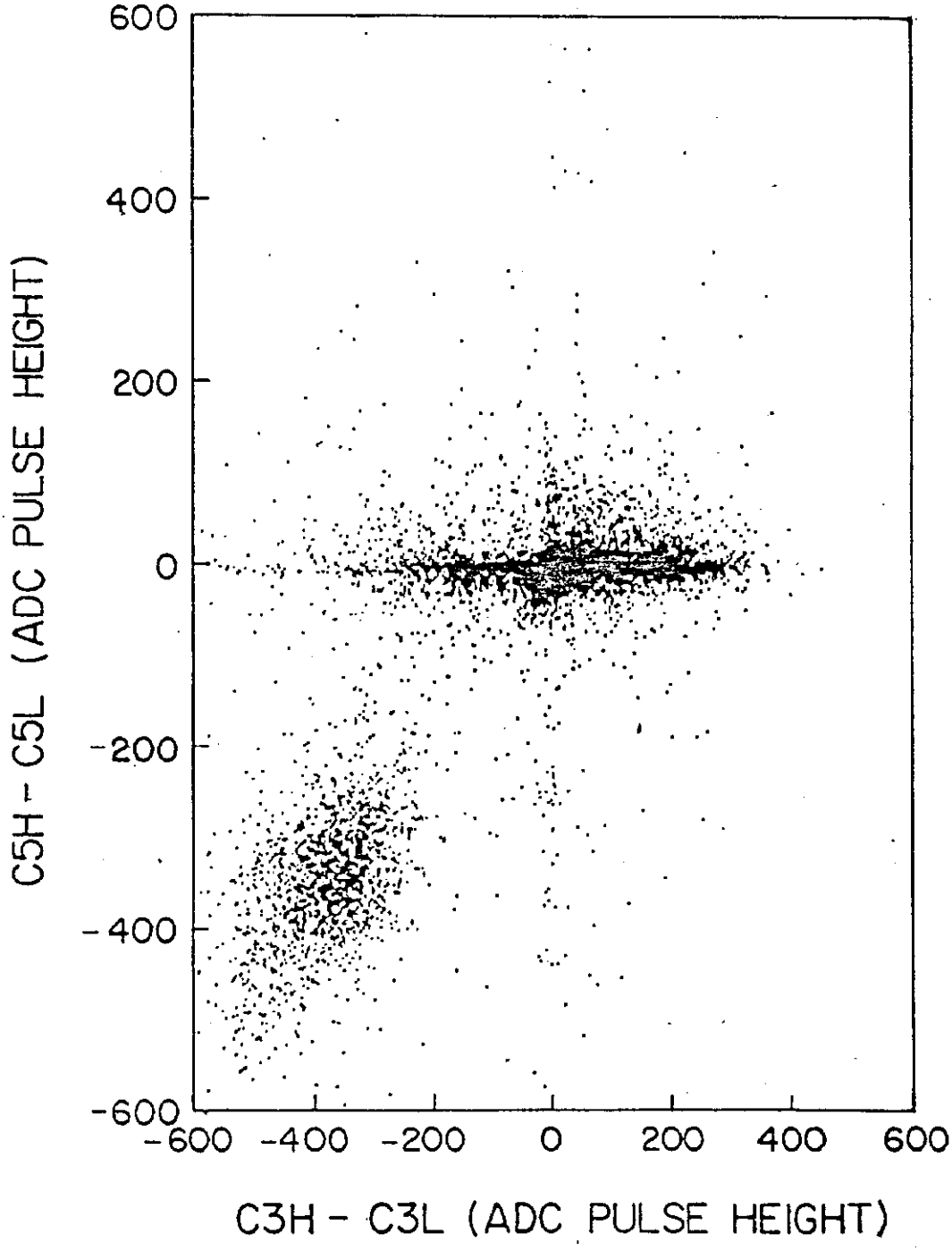
600
400
200
0
-200
-400
-600
-600 -400 -200 0 200 400 600
C5H - C5L (ADC PULSE HEIGHT)
C3H - C3L (ADC PULSE HEIGHT)

Fig. 18

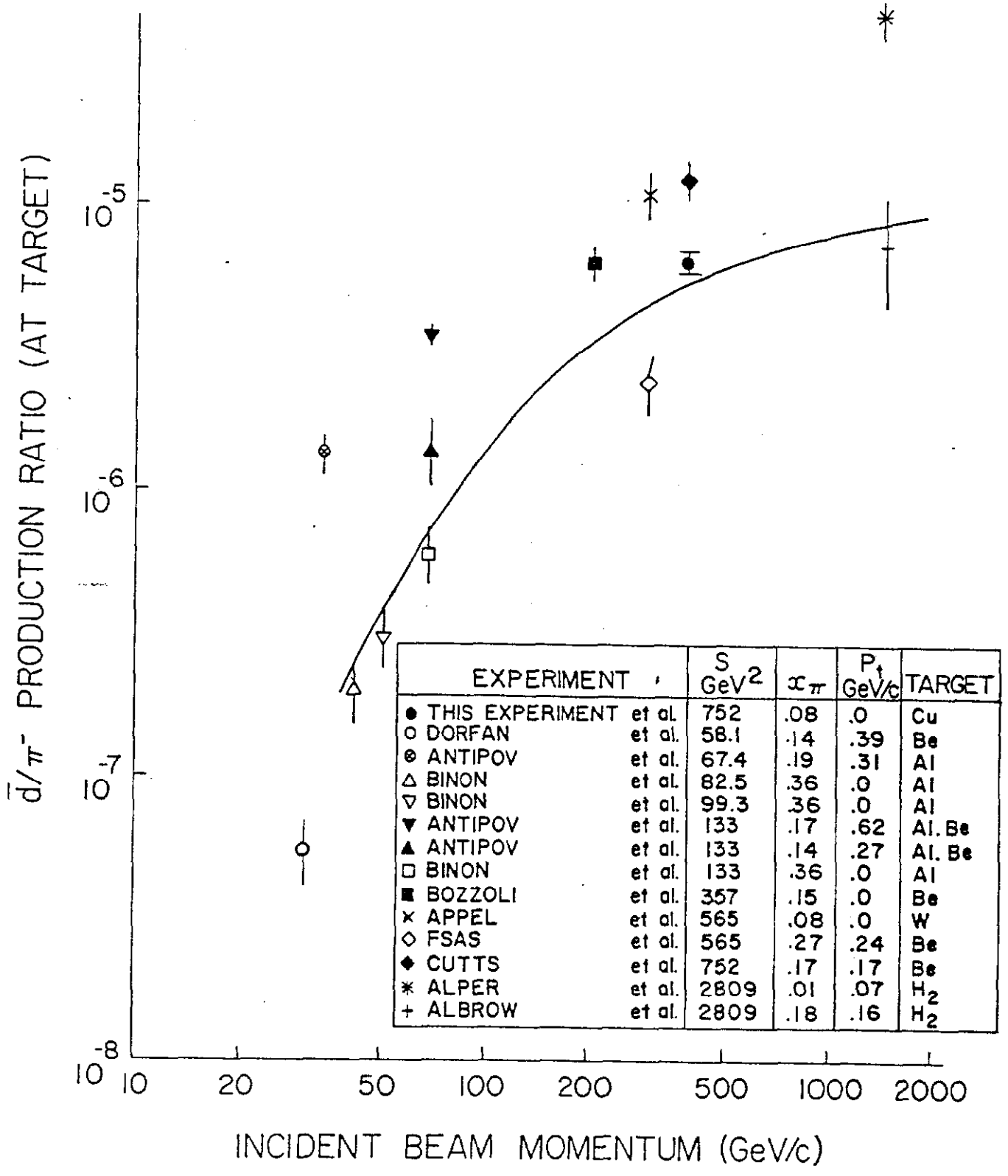
$\bar{d}/\pi^-$ PRODUCTION RATIO (AT TARGET)
10^{-5}
10^{-6}
10^{-7}
10^{-8}
10
20
50
100
200
500
1000
2000
INCIDENT BEAM MOMENTUM (GeV/c)
EXPERIMENT
S GeV^2
x_π
P_t GeV/c
TARGET
● THIS EXPERIMENT et al. 752 .08 .0 Cu
○ DORFAN et al. 58.1 .14 .39 Be
⊛ ANTIPOV et al. 67.4 .19 .31 Al
△ BINON et al. 82.5 .36 .0 Al
▽ BINON et al. 99.3 .36 .0 Al
▼ ANTIPOV et al. 133 .17 .62 Al. Be
▲ ANTIPOV et al. 133 .14 .27 Al. Be
□ BINON et al. 133 .36 .0 Al
■ BOZZOLI et al. 357 .15 .0 Be
× APPEL et al. 565 .08 .0 W
◇ FSAS et al. 565 .27 .24 Be
◆ CUTTS et al. 752 .17 .17 Be
✳ ALPER et al. 2809 .01 .07 H_2
+ ALBROW et al. 2809 .18 .16 H_2

Fig. 19

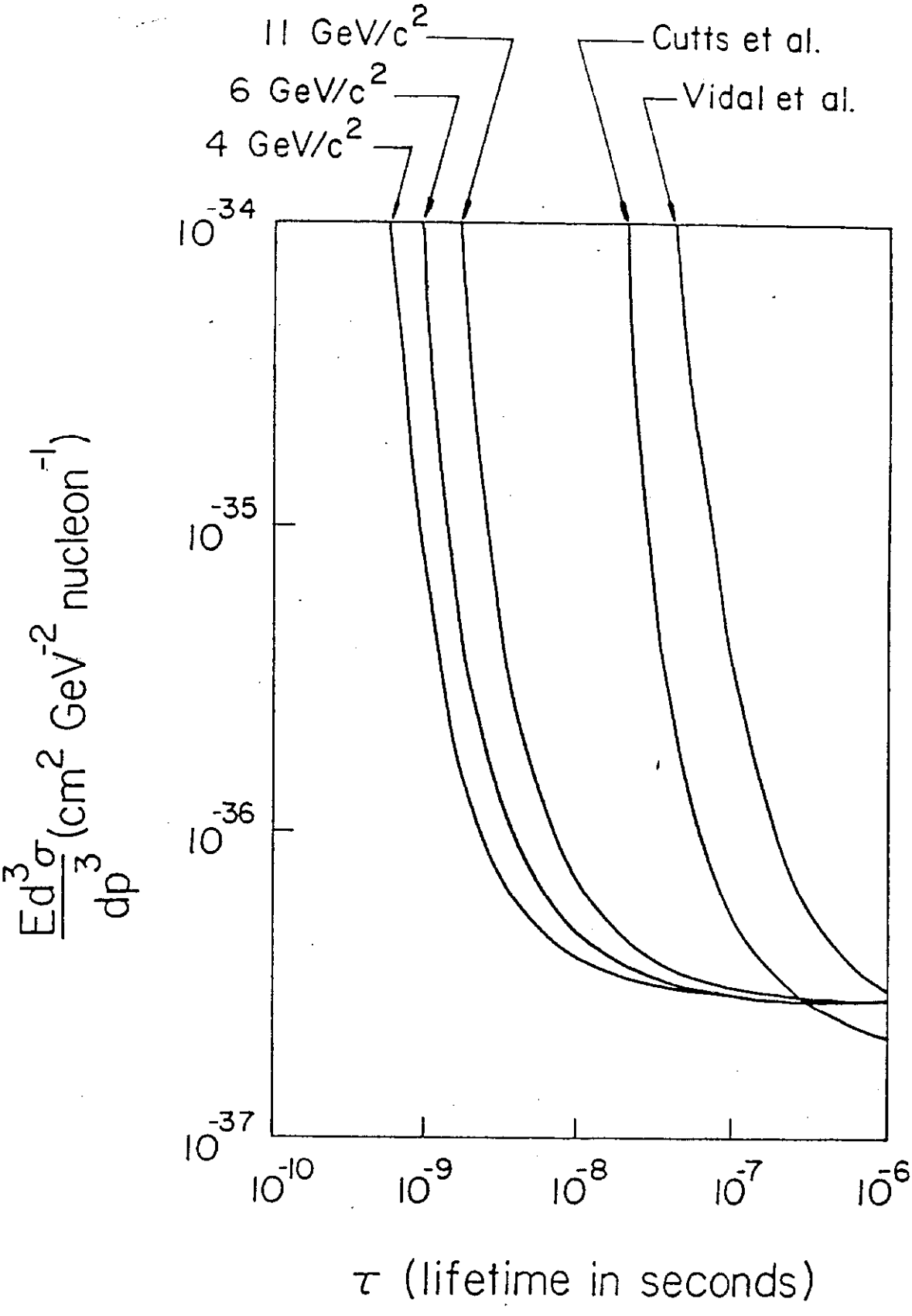
11 GeV/c²
6 GeV/c²
4 GeV/c²
Cutts et al.
Vidal et al.
10⁻³⁴
10⁻³⁵
10⁻³⁶
10⁻³⁷
10⁻¹⁰
10⁻⁹
10⁻⁸
10⁻⁷
10⁻⁶
Ed³σ/dp³ (cm² GeV⁻² nucleon⁻¹)
τ (lifetime in seconds)

Fig. 20

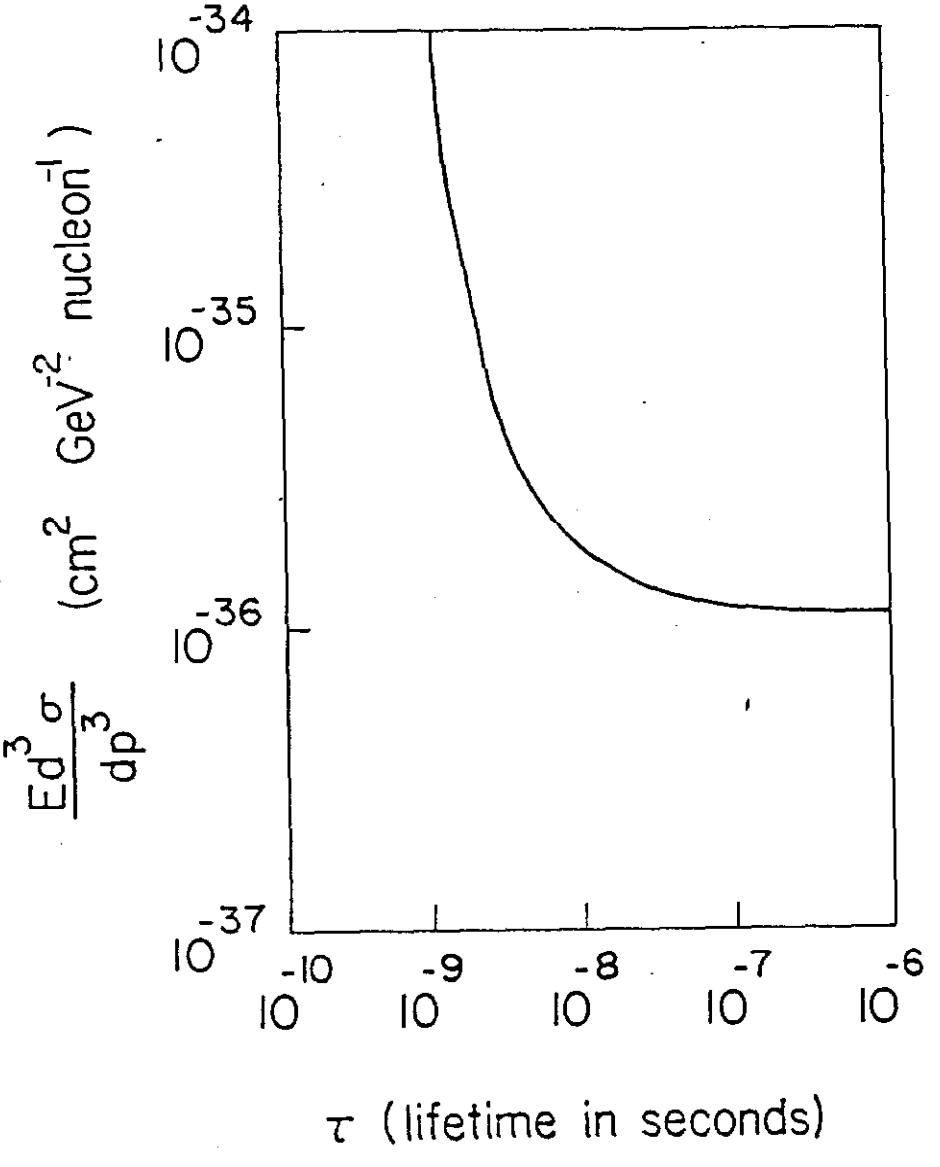
10^{-34}
10^{-35}
10^{-36}
10^{-37}
$\frac{Ed^3\sigma}{dp^3}$ (cm^2 GeV^{-2} nucleon^{-1})
10^{-10}
10^{-9}
10^{-8}
10^{-7}
10^{-6}
τ (lifetime in seconds)

Fig. 21

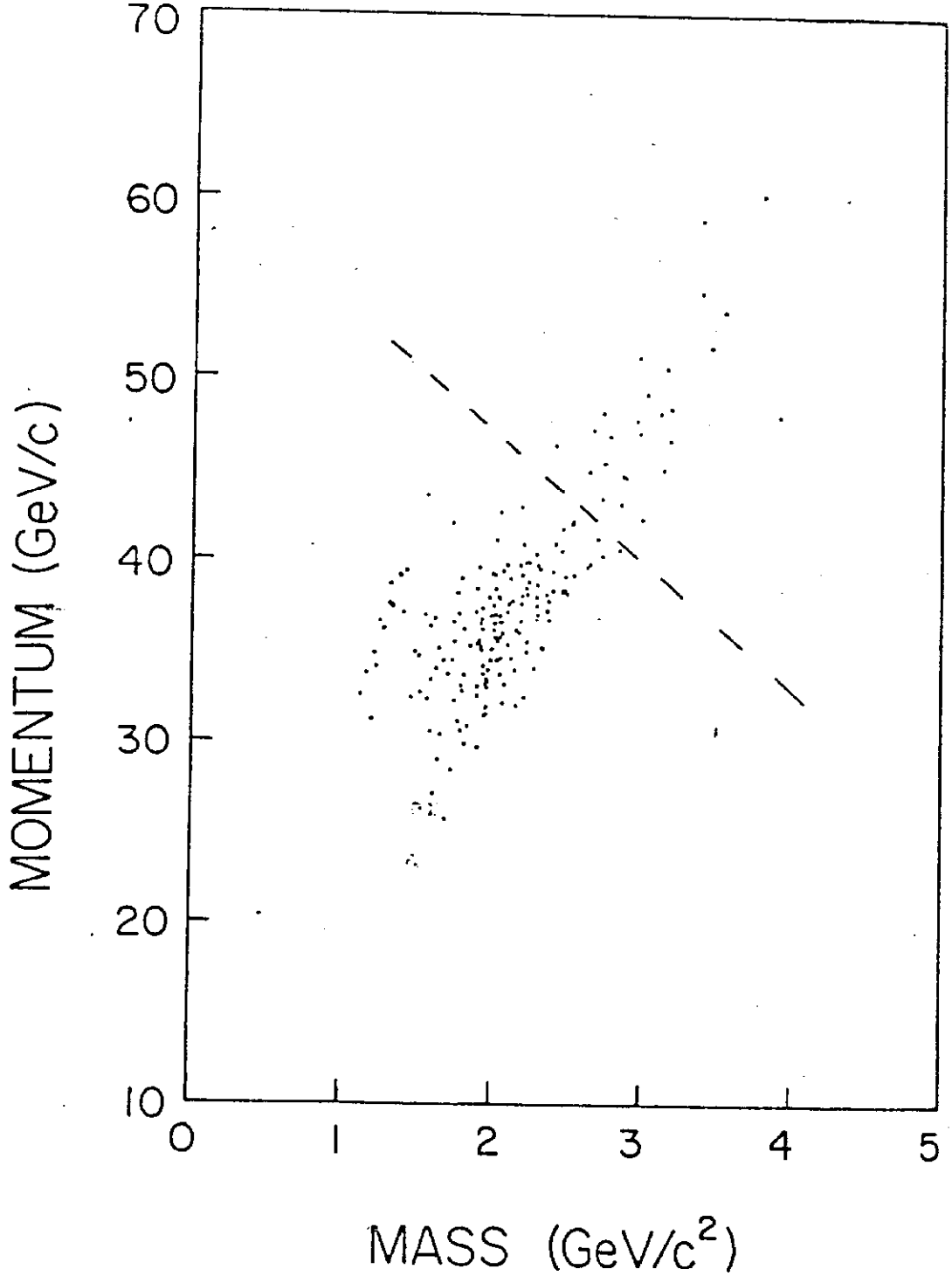

Fig. 22